Aerospace Science and Technology 130 (2022) 107917

Contents lists available at ScienceDirect

Aerospace Science and Technology

www.elsevier.com/locate/aescte

Robust distributed model predictive control for satellite cluster reconfiguration with collision avoidance

Siyuan Li, Dong Ye *, Yan Xiao, Zhaowei Sun

Research Center of Satellite Technology, Harbin Institute of Technology, Harbin 150001, China

ARTICLE INFO

Article history:
Received 24 June 2022
Received in revised form 12 September 2022
Accepted 26 September 2022
Available online 3 October 2022
Communicated by Chaoyong Li

Keywords:
Satellite cluster reconfiguration
Distributed model predictive control
Tube-based
Collision avoidance
Optimal allocation

ABSTRACT

This article investigates a reconfiguration problem of the satellite cluster with collision avoidance. Focusing on the uncertain disturbances with upper bound, a tube-based auxiliary controller is designed, which can improve the robustness of actual satellite cluster system. Then, a distributed model predictive controller (DMPC) is proposed for the nominal system with thrust constraints. In DMPC, the terminal constraints and terminal control law based on velocity obstacle are designed to satisfy the collision avoidance. Furthermore, the stability and feasibility can be ensured by using optimized slack variable. In addition, to reduce fuel consumption and the actions of collision, an optimal allocation strategy for target points based on Hungarian algorithm is adopted. Finally, the numerical simulations are presented to verify the effectiveness and advantage of the proposed scheme.

© 2022 Elsevier Masson SAS. All rights reserved.

1. Introduction

In recent years, the space industry has focused on the concept of distributed satellite system (DSS), which refers to a space system composed of multiple spacecrafts with same or different functions [1]. These spacecrafts cooperate with each other to realize the whole function of the space system [2]. With continuous practical research and experiments, distributed satellite system has converted from earth observation, navigation and communication services to the small-satellite revolution [3,4]. Satellite cluster is an important branch of DSS, which can carry a variety of payloads and accomplish complex space tasks through wireless communication network [5]. Compared to traditional monolithic satellites, satellite cluster has the characteristics of modularization, high flexibility and reliability [6]. In addition, satellite cluster not only has a short development cycle, but also causes lower manufacturing cost, which can satisfy the requirements of space missions more conveniently [7].

Although satellite cluster generally maintains a loose spatial configuration, the member satellites in cluster need to be reconfigured into a new spatial configuration when performing some specific space tasks, such as the observation of space targets [8]. In terms of control objectives, the reconfiguration of satellite cluster is the same as satellite formation. For satellite formation reconfiguration, the controller of each member satellite is usually designed independently using sliding mode control, adaptive control and other control methods [9–12]. However, the number of member satellites contained in the satellite cluster is large and collision avoidance needs to be considered in the whole control process. Therefore, distributed control is more suitable than centralized control and decentralized control.

During the reconfiguration of satellite cluster, collision avoidance not only exists within the cluster. The member satellites also need to avoid some space obstacles, such as space debris or non-cooperative targets [13]. The artificial potential field method is a classic collision avoidance method with clear physical meaning. The core idea is to define a scalar potential function artificially according to the desired states and the constraints of obstacles, so that the system states can converge to the desired states under the premise of avoiding collision [14]. However, the thruster carried by cluster satellite usually has an upper limit, the artificial potential field method may not fully guarantee collision avoidance. In addition, the artificial potential field method may have the problem of local optimal point. As a distributed control method, DMPC is widely used in multi-agent motion control because it can explicitly handle various constraints including collision avoidance and thrust constraints [15,16].

* Corresponding author.
E-mail address: yed@hit.edu.cn (D. Ye).

https://doi.org/10.1016/j.ast.2022.107917
1270-9638/© 2022 Elsevier Masson SAS. All rights reserved.

Considering collision avoidance, there have been many recent studies on satellite cluster reconfiguration using DMPC [17–20]. For the realization of large-scale satellite formations, L. Sauter proposed an analytic model predictive controller for fuel-minimized and collision-free trajectory following. Compared with the traditional integral-derivative type controller, the fuel consumption is greatly reduced [21]. Y. Lim presented a model predictive formation control based on an eccentricity/inclination vector separation strategy. In the optimization process, a simple objective function is designed to achieve alternate collision avoidance and real-time control. The constraint-tightening approach improves the robustness of the controller [22]. A decentralized model predictive control algorithm is proposed for the reconfiguration of spacecraft cluster consisting of hundreds of agents with limited capabilities by M. Daniel. Sequential convex programming has been used to determine collision-free, fuel-efficient spacecraft cluster reconfiguration trajectories and the model predictive control algorithms updated optimal trajectories during the whole process [23]. Considering the uncertainty and variability of targets motion, a DMPC controller is proposed by Z. Shi. The optimization objective is designed by the observation reward and the information gain of target distribution and a rolling optimization method is used to solve the established problem [24]. In these studies, DMPC controller handled collision avoidance constraints and thrust constraints well during the reconfiguration of satellite cluster, but few of them considered the effect of uncertain disturbances.

During the reconfiguration process, the satellites in cluster will be affected by various spatial disturbances. In addition to the space disturbances such as J_2 perturbation and atmospheric drag, the member satellites will be affected by some uncertain disturbances [25]. Although the model predictive controller has a certain inherent robustness, uncertain disturbances may lead to non-convergence of the system or make the control process unfeasible [26]. Aiming at this problem, J. Lofberg proposed a direct approach that calculated the optimal control sequence by adding the maximum disturbance sequence to the system [27]. However, this control strategy has two obvious drawbacks. The first one is that the maximum model predictive control is conservative. And the second one is that it is difficult to apply to engineering practice because of the huge amount of calculation. To improve these two problems, a tube-based robust model predictive control (RDMPC) has been studied by many scholars. D. Limón presented a robust tube-based model predictive controller for tracking of constrained linear systems with additive disturbances [28]. D.Q. Mayne extended this method to nonlinear systems and analyzed the advantages and disadvantages theoretically [29,30]. In the condition of bounded unknown disturbances, a method of decentralized tube-based model predictive control was applied to nonlinear multiagent systems by A. Nikou [31].

In general, DMPC is more suitable for the reconfiguration control of satellite cluster than traditional methods. It can not only deal with the constraints of collision avoidance and thrust amplitude directly, but also optimize the fuel consumption of satellite. However, the design of DMPC controller needs paying attention to some problems. First, when the initial distance error between the satellite in cluster and its target point is large, the distributed model prediction controller needs to choose a large prediction horizon or sampling time to make the terminal states in the robust invariant set, especially in the presence of space obstacles. In this case, the design of the terminal controller will also become complicated. On the other hand, unmodeled disturbances and system uncertainties not only reduce the accuracy of satellite cluster reconfiguration, but also affect the convergence of the DMPC controller.

Aiming at the above problems, the main contributions of this paper are summarized as follows: Firstly, a DMPC controller is designed for the nominal system considering collision avoidance and thruster amplitude constraints. By adopting slack variables and velocity obstacles, the collision avoidance of the nominal system can be guaranteed with a smaller prediction horizon or sampling time and the design of the terminal controller can be simplified at the same time. Secondly, to deal with the unknown disturbances of the actual system of the satellite cluster, a tube-based auxiliary controller is designed to compensate for the nominal system. Based on backstepping method, the errors between the actual system and the nominal system can be kept within a certain range related to the upper bound of the disturbance through a reasonable design of the control gains.

The structure of this paper is organized as follows. In Section 2, dynamics model of satellite cluster with J_2 perturbation and atmospheric drag is established to describe the accurate relative motion between satellites. For graph theory, some definitions are given. In Section 3, a robust distributed model predictive strategy for the satellite cluster reconfiguration is proposed. Through the analysis based on optimization theory, the stability and feasibility of the strategy are verified. Moreover, a target allocation method based on Hungarian algorithm is adopted to optimize the process of reconfiguration. In Section 4, numerical simulations are presented to verify the effectiveness of the controller. Finally, the summary of the main results is given in Section 5.

2. Problem formulation

2.1. Coordinate system

In order to describe the motion relationship between satellites conveniently, the relative motion dynamics equations of satellites are adopted. Before that, we usually define a satellite as a leader satellite and the other satellites are called follower satellites. Then two classical coordinate systems are established in Fig. 1, where O_E-XYZ is the ECI (Earth Centered Inertial) frame and the o-xyz is the LVLH (Local Vertical Local Horizon) frame.

2.2. Dynamics modeling

For the satellites orbit in low earth orbit, J_2 perturbation and atmospheric drag are two major disturbance factors. Therefore, it is necessary to consider these two disturbances for the relative motion dynamics model of the satellites. According to the Ref. [25], an accurate dynamics model of the satellites in ECI frame with J_2 perturbation and atmospheric drag is established as follows

$$\begin{aligned}
\dot{r} &= v_x \\
\dot{v}_x &= -\frac{\mu}{r^2} + \frac{h^2}{r^3} - \frac{k_{J_2}}{r^4}\left(1 - 3\sin^2 i \sin^2\theta\right) - k_a \left\|\boldsymbol{v}_{rel}\right\| v_x \\
\dot{h} &= -\frac{k_{J_2}}{r^3}\sin^2 i \sin 2\theta - k_a \left\|\boldsymbol{v}_{rel}\right\| \left(h - \omega_e r^2 \cos i\right)
\end{aligned}$$

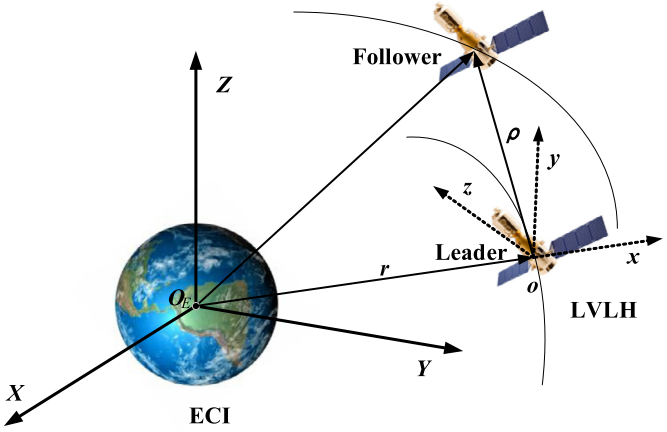

Fig. 1. Satellite coordinate system.

$$\begin{aligned}
\dot{\Omega} &= -\frac{k_{J_2}}{hr^3}\cos i \sin^2\theta - \frac{k_a}{2h}\left\|\boldsymbol{v}_{rel}\right\|\omega_e r^2 \sin 2\theta \\
\dot{i} &= -\frac{k_{J_2}}{2hr^3}\sin 2i \sin 2\theta - \frac{k_a}{h}\omega_e r^2 \sin i \cos^2\theta \\
\dot{\theta} &= \frac{h}{r^2} + \frac{2k_{J_2}}{hr^3}\cos^2 i \sin^2\theta + \frac{k_a}{2h}\omega_e r^2 \cos i \sin 2\theta
\end{aligned} \tag{1}$$

where r denotes the position vector of the satellite, v_x denotes the velocity in the direction of the position vector, h is the modulus of the orbital angular momentum, i is the orbit inclination, Ω is the right ascension of ascending node, and θ is the angle between the nodal line and position vector of the satellite. The coefficient of J_2 perturbation is expressed as $k_{J_2} = 3J_2\mu R_e/2$ where J_2 is the second harmonic coefficient of Earth, μ is the gravitational constant and R_e is the average radius of the Earth. $k_a = \frac{1}{2}C_d\frac{A}{m}\rho$ denotes the atmospheric resistance, where ρ is the atmospheric density. A denotes the effective area of the satellite relative to the atmosphere, m denotes the mass of the satellite, C_d denotes the pneumatic constant, and $\boldsymbol{v}_{rel}$ describes the relative velocity between satellite and atmosphere.

According to the Eq. (1), the dynamics model of the i-th follower satellite relative to the leader satellite in LVLH frame can be derived by the Lagrange equation. Then, the dynamics equation [25] can be obtained as follows

$$\begin{aligned}
\ddot{x}_i &= 2\dot{y}_i\omega_z - x_i\left(\eta_i^2 - \omega_z^2\right) + y_i\dot{\omega}_z - z_i\omega_x\omega_z - (\xi_i - \xi)\sin i \sin\theta \\
&\quad - r\left(\eta_i^2 - \eta^2\right) - k_{a,i}\left\|\boldsymbol{v}_{rel,i}\right\|(\dot{x}_i - y_i\omega_z) - \left(k_{a,i}\left\|\boldsymbol{v}_{rel,i}\right\| - k_a\left\|\boldsymbol{v}_{rel}\right\|\right)v_x \\
\ddot{y}_i &= -2\dot{x}_i\omega_z + 2\dot{z}_i\omega_x - x_i\dot{\omega}_z - y_i\left(\eta_i^2 - \omega_z^2 - \omega_x^2\right) + z_i\dot{\omega}_x - (\xi_i - \xi)\sin i\cos\theta \\
&\quad - k_{a,i}\left\|\boldsymbol{v}_{rel,i}\right\|(\dot{y}_i + x_i\omega_z - z_i\omega_x) - \left(k_{a,i}\left\|\boldsymbol{v}_{rel,i}\right\| - k_a\left\|\boldsymbol{v}_{rel}\right\|\right)\left(\frac{h}{r} - \omega_e\cos i\right) \\
\ddot{z}_i &= -2\dot{y}_i\omega_x - x_i\omega_x\omega_z - y_i\dot{\omega}_x - z_i\left(\eta_i^2 - \omega_x^2\right) - (\xi_i - \xi)\cos i \\
&\quad - k_{a,i}\left\|\boldsymbol{v}_{rel,i}\right\|(\dot{z}_i + y_i\omega_z) - \left(k_{a,i}\left\|\boldsymbol{v}_{rel,i}\right\| - k_a\left\|\boldsymbol{v}_{rel}\right\|\right)\omega_e r\sin i\cos\theta
\end{aligned} \tag{2}$$

where

$$\begin{aligned}
\xi &= \frac{2k_{J_2}}{r^4}\sin i\sin\theta \\
\xi_j &= \frac{2k_{J_2}}{r_j^5}\left((r + x_j)\sin i\sin\theta + y_j\sin i\cos\theta + z_j\cos i\right) \\
\eta^2 &= \frac{\mu}{r^3} + \frac{k_{J_2}}{r^5} - \frac{5k_{J_2}}{r^5}\sin^2 i\sin^2\theta \\
\eta_j^2 &= \frac{\mu}{r_j^3} + \frac{k_{J_2}}{r_j^5} - \frac{5k_{J_2}}{r_j^7}\left((r + x_j)\sin i\sin\theta + y_j\sin i\cos\theta + z_j\cos i\right)^2 \\
r_j &= \sqrt{(r + x_j)^2 + y_j^2 + z_j^2} \\
\omega_x &= \dot{i}\cos\theta + \dot{\Omega}\sin\theta\sin i \\
\omega_z &= \dot{\theta} + \dot{\Omega}\cos i
\end{aligned} \tag{3}$$

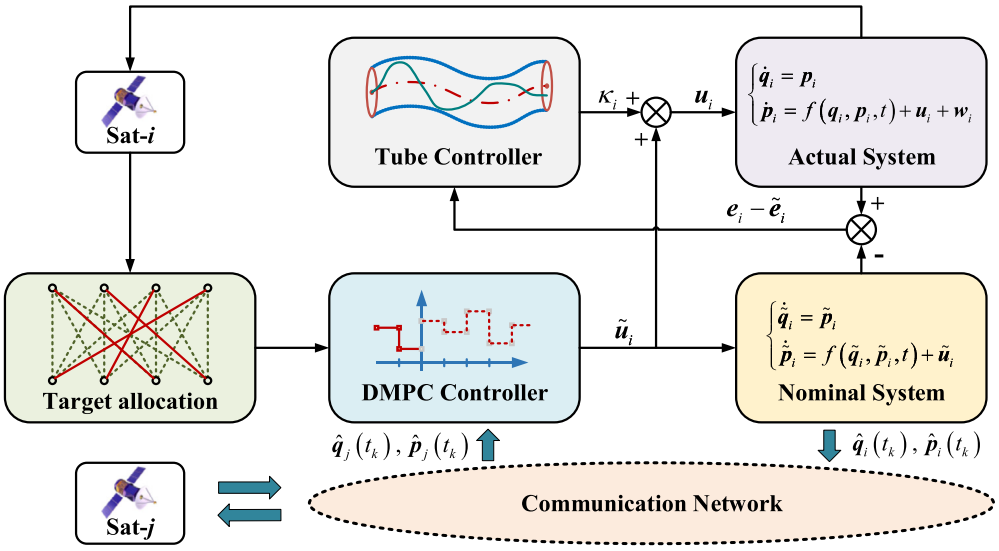

Fig. 2. Schematic diagram of satellite cluster reconfiguration control.

2.3. Network topology

For satellite cluster, the information exchange between satellites usually adopts wireless communication. Suppose that the communication links between satellites are bidirectional, the communication relationship between satellites can be represented by an undirected graph.

Define $G = (V, E, A)$ is an undirected graph with the set of nodes $V = \{v_1, v_2, \cdots, v_N\}$ and the set of edges $E \subseteq V \times V$. Adjacency matrix $A = (a_{ij})_{N\times N}$ represents the connection relationship between nodes. If there is an edge from v_i to v_j, the value of a_{ij} is equal to 1. Otherwise, the value of a_{ij} is equal to 0. In this paper, self-loop will not be considered, so that the diagonal element $a_{ii} = 0$.

In addition, it is defined that the maximum communication distance is r_c, and the safe distance between each satellite in cluster is r_s. Moreover, considering the limited communication resources, each satellite exchange information only with its nearest N_a satellites within the range of communication. In this way, it can not only ensure the connectivity of network topology of satellite cluster, but also save communication resources effectively.

2.4. Problem statement

Considering that the satellite cluster is made up of N satellites and a virtual satellite is set as the origin of LVLH coordinate system. Each satellite in cluster can obtain the states information of its neighbor satellites through wireless communication links. Define the position vector of the i-th satellite as $\boldsymbol{q}_i = [x_i, y_i, z_i]^{\mathrm{T}}$ and the velocity vector of the i-th satellite is $\boldsymbol{p}_i = [\dot{x}_i, \dot{y}_i, \dot{z}_i]^{\mathrm{T}}$. The actual dynamics model of the i-th satellite relative to the virtual reference satellite in LVLH coordinate can be written by Eq. (4).

$$\begin{cases} \dot{\boldsymbol{q}}_i = \boldsymbol{p}_i \\ \dot{\boldsymbol{p}}_i = f(\boldsymbol{q}_i, \boldsymbol{p}_i, t) + \boldsymbol{u}_i + \boldsymbol{w}_i \end{cases} \tag{4}$$

where, $f(\boldsymbol{q}_i, \boldsymbol{p}_i, t)$ is the dynamics equation of satellite cluster as Eq. (2) $\boldsymbol{u}_i = [u_{ix}, u_{iy}, u_{iz}]^{\mathrm{T}}$ denotes the actual control force vector of the i-th satellite. $\boldsymbol{w}_i$ represents uncertain disturbances including external disturbances, unmodeled dynamics or the loss of thruster.

Without considering uncertain disturbances, the nominal system of the satellite cluster can be expressed as

$$\begin{cases} \dot{\tilde{\boldsymbol{q}}}_i = \tilde{\boldsymbol{p}}_i \\ \dot{\tilde{\boldsymbol{p}}}_i = f(\tilde{\boldsymbol{q}}_i, \tilde{\boldsymbol{p}}_i, t) + \tilde{\boldsymbol{u}}_i \end{cases} \tag{5}$$

where $\tilde{\boldsymbol{q}}_i$ and $\tilde{\boldsymbol{p}}_i$ are the nominal position vector and nominal velocity vector of the i-th satellite, respectively. $f(\tilde{\boldsymbol{q}}_i, \tilde{\boldsymbol{p}}_i, t)$ is the nonlinear item resulting from the nominal states and $\tilde{\boldsymbol{u}}_i$ is the nominal control force vector.

During the reconfiguration of satellite cluster, multiple satellites may be needed to be evenly distributed around a target spacecraft. The schematic diagram of satellite cluster reconfiguration control is in Fig. 2.

Before controlling the member satellites, the Hungarian algorithm is used to optimize the allocation between satellites and target points. Then, the DMPC controller will solve the target tracking problem considering collision avoidance for the nominal system of each satellite. Finally, in order to compensate the uncertain disturbances, a tube-based auxiliary controller is designed. The combination of the auxiliary controller and the DMPC controller constitutes the controller of the actual system, under the action of which the satellite cluster can realize the reconfiguration safely.

3. Controller design

In this section, a satellite cluster control strategy based on robust distributed model predictive control (RDMPC) is discussed. Firstly, a tube-based auxiliary controller is designed for satellite cluster system with uncertain disturbances. Then, a DMPC controller is proposed

for the nominal system of the actual system considering thrust constraints and collision avoidance. Meanwhile, the communication limit of each satellite in the cluster is considered. In addition, a target allocation algorithm based on Hungarian algorithm is adopted for tracking the targets reasonably.

3.1. Tube-based auxiliary controller of satellite cluster with uncertain disturbance

From Section 2.4, the actual dynamics model of the i-th satellite in cluster is

$$\begin{cases} \dot{\boldsymbol{q}}_i = \boldsymbol{p}_i \\ \dot{\boldsymbol{p}}_i = f\left(\boldsymbol{q}_i, \boldsymbol{p}_i, t\right) + \boldsymbol{u}_i + \boldsymbol{w}_i \end{cases} \tag{6}$$

It is worth noting that the lower bound of $\boldsymbol{w}_i$ is zero, indicating that there is no uncertain disturbance. For the upper bound, $\boldsymbol{w}_i$ should be smaller than the difference between the maximum magnitude of the thruster and the system dynamics $f\left(\boldsymbol{q}_i, \boldsymbol{p}_i, t\right)$. Otherwise, no matter how the control law is designed, the control of the satellite cluster cannot be realized. Therefore, suppose that there exists a finite constant $\overline{\boldsymbol{w}}_i < \sup\left(\left\|\boldsymbol{u}_i - f\left(\boldsymbol{q}_i, \boldsymbol{p}_i, t\right)\right\|\right)$ such that

$$\boldsymbol{w}_i \in \boldsymbol{W}_i := \left\{\boldsymbol{w}_i \in \mathbf{R}^n : \|\boldsymbol{w}_i\| \leq \overline{\boldsymbol{w}}_i\right\} \quad \forall t \in \mathbf{R} \geq 0,\ i \in G \tag{7}$$

During the reconfiguration of satellite cluster, $\boldsymbol{q}_{id} = [x_{id}, y_{id}, z_{id}]^{\mathrm{T}}$ and $\boldsymbol{p}_{id} = [\dot{x}_{id}, \dot{y}_{id}, \dot{z}_{id}]^{\mathrm{T}}$ denote the desired position vector and desired velocity vector of the i-th satellite, respectively. According to Eq. (4) and Eq. (5), define the actual error as

$$\boldsymbol{e}_i = \begin{bmatrix} \boldsymbol{e}_{i1} \\ \boldsymbol{e}_{i2} \end{bmatrix} = \begin{bmatrix} \boldsymbol{q}_i - \boldsymbol{q}_{id} \\ \boldsymbol{p}_i - \boldsymbol{p}_{id} \end{bmatrix} \tag{8}$$

and the nominal error as

$$\tilde{\boldsymbol{e}}_{\boldsymbol{i}} = \begin{bmatrix} \tilde{\boldsymbol{e}}_{i1} \\ \tilde{\boldsymbol{e}}_{i2} \end{bmatrix} = \begin{bmatrix} \tilde{\boldsymbol{q}}_i - \boldsymbol{q}_{id} \\ \tilde{\boldsymbol{p}}_i - \boldsymbol{p}_{id} \end{bmatrix} \tag{9}$$

Let

$$\boldsymbol{\varepsilon}_i = \boldsymbol{e}_{i1} - \tilde{\boldsymbol{e}}_{i1} = \boldsymbol{q}_i - \tilde{\boldsymbol{q}}_i \tag{10}$$

By using Eq. (8), Eq. (9) and Eq. (10), the deviation of $\boldsymbol{\varepsilon}_i$ can be given by

$$\begin{cases} \dot{\boldsymbol{\varepsilon}}_i = \dot{\boldsymbol{e}}_{i1} - \dot{\tilde{\boldsymbol{e}}}_{i1} = \boldsymbol{e}_{i2} - \tilde{\boldsymbol{e}}_{i2} = \boldsymbol{p}_i - \tilde{\boldsymbol{p}}_i \\ \ddot{\boldsymbol{\varepsilon}}_i = \dot{\boldsymbol{e}}_{i2} - \dot{\tilde{\boldsymbol{e}}}_{i2} = f\left(\boldsymbol{q}_i, \boldsymbol{p}_i, t\right) - f\left(\tilde{\boldsymbol{q}}_i, \tilde{\boldsymbol{p}}_i, t\right) + \left(\boldsymbol{u}_i - \tilde{\boldsymbol{u}}_i\right) + \boldsymbol{w}_i \end{cases} \tag{11}$$

Suppose that $\boldsymbol{u}_i = \tilde{\boldsymbol{u}}_i + \kappa_i\left(\boldsymbol{p}_i, \tilde{\boldsymbol{p}}_i, \boldsymbol{q}_i, \tilde{\boldsymbol{q}}_i\right)$ where $\kappa_i\left(\boldsymbol{p}_i, \tilde{\boldsymbol{p}}_i, \boldsymbol{q}_i, \tilde{\boldsymbol{q}}_i\right)$ is the auxiliary control law.

Lemma 1. *For any vectors $x, y \in \mathbf{R}^n$, positive definite matrix $Q \in \mathbf{R}^{n\times n}$ and constant $\eta > 0$, it holds that*

$$x^{\mathrm{T}} Q\, y \leq \frac{1}{4\eta} x^{\mathrm{T}} Q\, x + \eta\, y^{\mathrm{T}} Q\, y \tag{12}$$

Theorem 1. *The expression of the auxiliary control law is designed as*

$$\boldsymbol{\kappa}_i\left(\boldsymbol{p}_i, \tilde{\boldsymbol{p}}_i, \boldsymbol{q}_i, \tilde{\boldsymbol{q}}_i\right) = -f\left(\boldsymbol{q}_i, \boldsymbol{p}_i, t\right) + f\left(\tilde{\boldsymbol{q}}_i, \tilde{\boldsymbol{p}}_i, t\right) - \left(1 + k_{i1}\right)\boldsymbol{\varepsilon}_i - \left(k_{i1} + k_{i2}\right)\dot{\boldsymbol{\varepsilon}}_i \tag{13}$$

and the control gains k_{i1} and k_{i2} are chosen as

$$\begin{cases} k_{i1} > 0 \\ k_{i2} \geq \dfrac{1}{4\eta_i} \end{cases} \tag{14}$$

where $\eta_i > 0$. For Eq. (10), the sets of errors ranges can be obtained as

$$\Phi_i = \left\{\boldsymbol{\varepsilon}_i(t) \in \mathbf{R}^n : \|\boldsymbol{\varepsilon}_i(t)\| \leq \overline{\boldsymbol{\varepsilon}}_i := \sqrt{\frac{\eta_i}{k_{i1}}}\,\overline{\boldsymbol{w}}_i,\ \forall t \in \mathbf{R} \geq 0\right\} \tag{15}$$

Proof. Choose a Lyapunov function candidate as

$$V_{i1} = \frac{1}{2}\boldsymbol{\varepsilon}_i^{\mathrm{T}}\boldsymbol{\varepsilon}_i \tag{16}$$

Obviously, V_{i1} is positive definite with $V_{i1}(0) = 0$. The derivative of V_i is given by Eq. (17)

$$\dot{V}_{i1} = \boldsymbol{\varepsilon}_i^{\mathrm{T}}\dot{\boldsymbol{\varepsilon}}_i \tag{17}$$

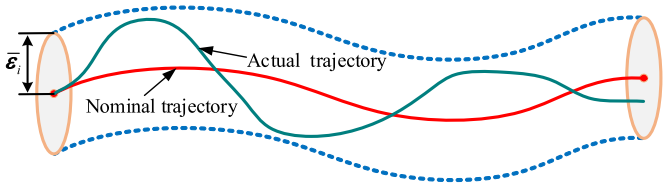

Fig. 3. The actual trajectory under the tube-based auxiliary controller.

If $\dot{V}_{i1}$ is expected to be negative definite, then the $\dot{\boldsymbol{\varepsilon}}_{id}$ which is the expected value of $\dot{\boldsymbol{\varepsilon}}_i$ can be chosen as $\dot{\boldsymbol{\varepsilon}}_{id} = -k_{i1}\boldsymbol{\varepsilon}_i$. Define $\boldsymbol{\delta}_i = \dot{\boldsymbol{\varepsilon}}_i - \dot{\boldsymbol{\varepsilon}}_{id}$. Then, Eq. (17) can be further derived as

$$\dot{V}_{i1} = \boldsymbol{\varepsilon}_i^{\mathrm{T}}\left(\dot{\boldsymbol{\varepsilon}}_{id} + \boldsymbol{\delta}_i\right) = -k_{i1}\boldsymbol{\varepsilon}_i^{\mathrm{T}}\boldsymbol{\varepsilon}_i + \boldsymbol{\varepsilon}_i^{\mathrm{T}}\boldsymbol{\delta}_i \tag{18}$$

According to Eq. (11), the derivative of $\boldsymbol{\delta}_i$ can be expressed as

$$\begin{aligned}\dot{\boldsymbol{\delta}}_i &= \ddot{\boldsymbol{\varepsilon}}_i - \ddot{\boldsymbol{\varepsilon}}_{id} \\ &= f\left(\boldsymbol{q}_i, \boldsymbol{p}_i, t\right) - f\left(\tilde{\boldsymbol{q}}_i, \tilde{\boldsymbol{p}}_i, t\right) + \kappa_i + \boldsymbol{w}_i + k_{i1}\dot{\boldsymbol{\varepsilon}}_i\end{aligned} \tag{19}$$

Choose another Lyapunov function candidate as

$$V_{i2} = V_{i1} + \frac{1}{2}\boldsymbol{\delta}_i^{\mathrm{T}}\boldsymbol{\delta}_i \tag{20}$$

The derivative of V_{i2} can be obtained as

$$\begin{aligned}\dot{V}_{i2} &= -k_{i1}\boldsymbol{\varepsilon}_i^{\mathrm{T}}\boldsymbol{\varepsilon}_i + \boldsymbol{\varepsilon}_i^{\mathrm{T}}\boldsymbol{\delta}_i + \boldsymbol{\delta}_i^{\mathrm{T}}\dot{\boldsymbol{\delta}}_i \\ &= -k_{i1}\boldsymbol{\varepsilon}_i^{\mathrm{T}}\boldsymbol{\varepsilon}_i + \boldsymbol{\delta}_i^{\mathrm{T}}\left(\dot{\boldsymbol{\delta}}_i + \boldsymbol{\varepsilon}_i\right) \\ &= -k_{i1}\boldsymbol{\varepsilon}_i^{\mathrm{T}}\boldsymbol{\varepsilon}_i + \boldsymbol{\delta}_i^{\mathrm{T}}\left(f\left(\boldsymbol{q}_i, \boldsymbol{p}_i, t\right) - f\left(\tilde{\boldsymbol{q}}_i, \tilde{\boldsymbol{p}}_i, t\right) + \kappa_i + \boldsymbol{w}_i + k_{i1}\dot{\boldsymbol{\varepsilon}}_i + \boldsymbol{\varepsilon}_i\right)\end{aligned} \tag{21}$$

According to the conditions in Theorem 1 and Lemma 1, it yields

$$\begin{aligned}\dot{V}_{i2} &= -k_{i1}\boldsymbol{\varepsilon}_i^{\mathrm{T}}\boldsymbol{\varepsilon}_i - k_{i2}\boldsymbol{\delta}_i^{\mathrm{T}}\boldsymbol{\delta}_i + \boldsymbol{\delta}_i^{\mathrm{T}}\boldsymbol{w}_i \\ &\le -k_{i1}\boldsymbol{\varepsilon}_i^{\mathrm{T}}\boldsymbol{\varepsilon}_i - k_{i2}\boldsymbol{\delta}_i^{\mathrm{T}}\boldsymbol{\delta}_i + \boldsymbol{\delta}_i^{\mathrm{T}}\boldsymbol{w}_i \\ &\le -k_{i1}\boldsymbol{\varepsilon}_i^{\mathrm{T}}\boldsymbol{\varepsilon}_i - k_{i2}\boldsymbol{\delta}_i^{\mathrm{T}}\boldsymbol{\delta}_i + \frac{1}{4\eta_i}\boldsymbol{\delta}_i^{\mathrm{T}}\boldsymbol{\delta}_i + \eta_i\boldsymbol{w}_i^{\mathrm{T}}\boldsymbol{w}_i \\ &\le -k_{i1}\boldsymbol{\varepsilon}_i^{\mathrm{T}}\boldsymbol{\varepsilon}_i - \left(k_{i2} - \frac{1}{4\eta_i}\right)\boldsymbol{\delta}_i^{\mathrm{T}}\boldsymbol{\delta}_i + \eta_i\boldsymbol{w}_i^{\mathrm{T}}\boldsymbol{w}_i\end{aligned} \tag{22}$$

If choose $k_{i2} \ge \frac{1}{4\eta_i}$, Eq. (22) can be simplified as

$$\dot{V}_{i2} \le -k_{i1}\boldsymbol{\varepsilon}_i^{\mathrm{T}}\boldsymbol{\varepsilon}_i + \eta_i\boldsymbol{w}_i^{\mathrm{T}}\boldsymbol{w}_i \tag{23}$$

Therefore, if $k_{i1} > 0$, it can be guaranteed that $\dot{V}_{i2} \le 0$ when $\|\boldsymbol{\varepsilon}_i(t)\| \ge \bar{\boldsymbol{\varepsilon}}_i$, where $\bar{\boldsymbol{\varepsilon}}_i$ is given by Eq. (15). Because of $\|\boldsymbol{\varepsilon}_i(0)\| = 0$, it gets

$$\|\boldsymbol{\varepsilon}_i(t)\| \le \bar{\boldsymbol{\varepsilon}}_i,\ \forall t \in \mathbf{R} \ge 0,\ i \in G \quad \square \tag{24}$$

To sum up, the auxiliary controller can keep the distance error between actual and nominal trajectories within a bounded range which is related to the upper bound of the uncertain disturbance. The schematic diagram is shown in Fig. 3.

3.2. DMPC controller design

For large scale satellite clusters, centralized control strategy may lead to communication congestion which is obviously unsuitable. Therefore, a DMPC controller is designed for the satellite cluster in this section. For the DMPC controller, three control objectives should be concerned. The first one is to let each satellite track its target point. The second one is to ensure that there is no collision between satellites in cluster based on the predictive information of the neighbor satellites. The last one is that all satellites maintain a safe distance from the target spacecraft and space obstacle during the control process.

According to Section 2.4, the nominal system of satellite cluster is expressed as

$$\begin{cases}\dot{\tilde{\boldsymbol{q}}}_i = \tilde{\boldsymbol{p}}_i \\ \dot{\tilde{\boldsymbol{p}}}_i = f\left(\tilde{\boldsymbol{q}}_i, \tilde{\boldsymbol{p}}_i, t\right) + \tilde{\boldsymbol{u}}_i\end{cases} \tag{25}$$

where $\tilde{\boldsymbol{q}}_i$ is the nominal position vector and $\tilde{\boldsymbol{p}}_i$ is the nominal velocity vector of the i-th satellite. $\tilde{\boldsymbol{u}}_i$ is the nominal control force. $\boldsymbol{q}_{id}$ and $\boldsymbol{p}_{id}$ are the desired position vector and desired velocity vector of the i-th satellite. In this article, the desired velocity vector is assumed to be $\boldsymbol{p}_{id} = [0\ 0\ 0]^{\mathrm{T}}$.

Suppose that the topology of the nominal system is an undirected graph $G = (V, E, A)$ and the set of neighbor satellites of the i-th satellite is $\boldsymbol{N}_a$. Define $\boldsymbol{\zeta}_i = \left[\tilde{\boldsymbol{q}}_i^{\mathrm{T}}, \tilde{\boldsymbol{p}}_i^{\mathrm{T}}\right]^{\mathrm{T}}$, $\boldsymbol{\zeta}_{id} = \left[\boldsymbol{q}_{id}^{\mathrm{T}}, \boldsymbol{p}_{id}^{\mathrm{T}}\right]^{\mathrm{T}}$, $\boldsymbol{\zeta}_{-i} = \left[\boldsymbol{\zeta}_{j_1}^{\mathrm{T}}, \boldsymbol{\zeta}_{j_2}^{\mathrm{T}}, \ldots, \boldsymbol{\zeta}_{j_k}^{\mathrm{T}}\right]^{\mathrm{T}}$ is the vector consisting of the states of all the neighbor satellites of the i-th satellite, where $j_k \in \boldsymbol{N}_a$.

For the DMPC controller, T_p is the prediction horizon and Δt is the sampling period which is the time interval between two adjacent sampling instants t_k and t_{k+1}. And it is considered that a prediction horizon contains m_p sampling times. Since all terms in Eq. (25) can be obtained at time t_k, the nominal system under the control force $\tilde{\boldsymbol{u}}_i$ can be described as

$$\boldsymbol{\zeta}_i\left(t_k + \Delta t \mid t_k\right) = g\left(\boldsymbol{\zeta}_i\left(t_k \mid t_k\right), \tilde{\boldsymbol{u}}_i, \Delta t\right) \tag{26}$$

where $g\left(\boldsymbol{\zeta}_i\left(t_k \mid t_k\right), \tilde{\boldsymbol{u}}_i, \Delta t\right)$ is the function obtained by integrating Eq. (25). During a sampling period, it is considered that $\tilde{\boldsymbol{u}}_i$ provides a constant thrust. Based on this, the cost function of the nominal system can be described as

$$J_i\left(t_k, \boldsymbol{\zeta}_i, \boldsymbol{\zeta}_{-i}, \boldsymbol{\zeta}_{id}, \tilde{\boldsymbol{u}}_i, \lambda_i\right) = \sum_{m=0}^{m_p-1} J_i^H\left(t_k + m\Delta t \mid t_k, \boldsymbol{\zeta}_i, \boldsymbol{\zeta}_{-i}, \boldsymbol{\zeta}_{id}, \tilde{\boldsymbol{u}}_i\right) + \sum_{m=0}^{m_p-1} J_i^Q\left(t_k + m\Delta t \mid t_k, \lambda_i\right) \tag{27}$$

where $J_i^H\left(t_k + m\Delta t \mid t_k, \boldsymbol{\zeta}_i, \boldsymbol{\zeta}_{-i}, \boldsymbol{\zeta}_{id}, \tilde{\boldsymbol{u}}_i\right)$ is the cost function contains both tracking error and fuel consumption and $J_i^Q\left(t_k + m\Delta t \mid t_k, \lambda_i\right)$ is the cost of slack variable λ_i. Based on coefficients α_i, β_i and γ_i, the J_i^H and J_i^Q can be described as follows

$$\begin{cases} J_i^H\left(t_k + m\Delta t \mid t_k, \boldsymbol{\zeta}_i, \boldsymbol{\zeta}_{-i}, \boldsymbol{\zeta}_{id}, \tilde{\boldsymbol{u}}_i\right) = \alpha_i \left\|\tilde{\boldsymbol{q}}_i\left(t_k + m\Delta t \mid t_k\right) - \boldsymbol{q}_{id}\right\|^2 + \beta_i \left\|\tilde{\boldsymbol{u}}_i\left(t_k + m\Delta t \mid t_k\right)\right\|^2 \\ J_i^Q\left(t_k + m\Delta t \mid t_k, \lambda_i\right) = \gamma_i \left\|\lambda_i\left(t_k + m\Delta t \mid t_k\right)\right\|^2 \end{cases} \tag{28}$$

Define the optimal control sequence at t_k is $\boldsymbol{u}_i^*\left(t_k + m\Delta t \mid t_k\right)$, $m = 0, 1, \cdots, m_p - 1$. Then, the optimal prediction states of the nominal system can be computed as $\boldsymbol{\zeta}_i^*\left(t_k + m\Delta t \mid t_k\right)$, $m = 0, 1, \cdots, m_p - 1$. Then only the first item of $\boldsymbol{u}_i^*\left(t_k + m\Delta t \mid t_k\right)$ will be applied to the system.

In addition, since the actual state information of the neighbor satellites at the next moment cannot be computed at the current moment, the predicted state information of the neighbor satellite should be used as the basis of collision avoidance. Define the predictive control sequence as

$$\hat{\boldsymbol{u}}_i\left(t_k + m\Delta t \mid t_k\right) = \begin{cases} \boldsymbol{u}_i^*\left(t_k + m\Delta t \mid t_{k-1}\right), & m = 0, 1, \cdots, m_p - 2 \\ \boldsymbol{\rho}_i\left(\boldsymbol{\zeta}_i^*\left(t_k + \left(m_p - 1\right)\Delta t \mid t_{k-1}\right)\right), & m = m_p - 1 \end{cases} \tag{29}$$

where $\boldsymbol{\rho}_i\left(\boldsymbol{\zeta}_i^*\left(t_k - 1 + m_p \mid t_{k-1}\right)\right)$ is the terminal controller to be designed later. Further, the predictive states of satellites in nominal system can be calculated as

$$\hat{\boldsymbol{\zeta}}_i\left(t_k + m\Delta t \mid t_k\right) = \begin{cases} \boldsymbol{\zeta}_i^*\left(t_k + m\Delta t \mid t_{k-1}\right), & m = 0, 1, \cdots, m_p - 1 \\ \boldsymbol{\zeta}_i^{\rho}\left(t_k + m_p\Delta t \mid t_{k-1}\right), & m = m_p \end{cases} \tag{30}$$

where $\boldsymbol{\zeta}_i^{\rho}\left(t_k + m_p\Delta t \mid t_{k-1}\right)$ is the terminal state which is calculated by $\boldsymbol{\rho}_i\left(\boldsymbol{\zeta}_i^*\left(t_k - 1 + m_p \mid t_{k-1}\right)\right)$. For collision avoidance and obstacle avoidance, the satellites in cluster should maintain the following constraints

$$\begin{cases} \left\|\boldsymbol{q}_i\left(t_k + m\Delta t \mid t_k\right) - \boldsymbol{q}_j\left(t_k + m\Delta t \mid t_k\right)\right\| \geq 2r_s,\ i, j \in V,\ m = 0, 1, \cdots, m_p - 1 \\ \left\|\boldsymbol{q}_i\left(t_k + m\Delta t \mid t_k\right) - \boldsymbol{q}_{obs}\left(t_k + m\Delta t \mid t_k\right)\right\| \geq r_s + r_{obs},\ i \in V,\ m = 0, 1, \cdots, m_p - 1 \end{cases} \tag{31}$$

where $\boldsymbol{q}_{obs}$ is the position vector of the space obstacle. r_s and r_{obs} are the safe distances of satellites and obstacle, respectively. According to the nominal system and the communication topology G, a DMPC controller with collision and obstacle avoidance constraints can be formulated as follows

$$J_i^*\left(\boldsymbol{\zeta}_i^*, \boldsymbol{u}_i^*, t_k\right) = \min_{\tilde{\boldsymbol{u}}_i} J_i\left(t_k, \boldsymbol{\zeta}_i, \boldsymbol{\zeta}_{-i}, \boldsymbol{\zeta}_{id}, \tilde{\boldsymbol{u}}_i, \eta_i\right)$$

s.t.

$$\begin{aligned} &\boldsymbol{\zeta}_i\left(t_k + (m+1)\Delta t \mid t_k\right) = g\left(\boldsymbol{\zeta}_i\left(t_k + m\Delta t \mid t_k\right), \tilde{\boldsymbol{u}}_i, \Delta t\right) \\ &\boldsymbol{\zeta}_i\left(t_k + m\Delta t \mid t_k\right) \in \boldsymbol{\Xi}_i \\ &\boldsymbol{\zeta}_i\left(t_k + m_p\Delta t \mid t_k\right) \in \boldsymbol{\Xi}_{if} \\ &\tilde{\boldsymbol{u}}_i\left(t_k + m\Delta t \mid t_k\right) \in \mathbf{U}_i \ominus \sup\{\boldsymbol{\kappa}_i\} \\ &\left\|\boldsymbol{q}_i\left(t_k + m\Delta t \mid t_k\right) - \boldsymbol{q}_j\left(t_k + m\Delta t \mid t_k\right)\right\| \geq 2r_s \\ &\left\|\boldsymbol{q}_i\left(t_k + m\Delta t \mid t_k\right) - \boldsymbol{q}_{obs}\left(t_k + m\Delta t \mid t_k\right)\right\| \geq r_s + r_{obs} \\ &V_i\left(t_k + (m+1)\Delta t \mid t_k, \boldsymbol{\zeta}_i, \boldsymbol{\zeta}_{id}\right) - V_i\left(t_k + m\Delta t \mid t_k, \boldsymbol{\zeta}_i, \boldsymbol{\zeta}_{id}\right) \\ &\quad \leq -\left(\sigma_i - \lambda_i\left(t_k + m\Delta t \mid t_k\right)\right) V_i\left(t_k + m\Delta t \mid t_k, \boldsymbol{\zeta}_i, \boldsymbol{\zeta}_{id}\right) \\ &\lambda_i\left(t_k + m\Delta t \mid t_k\right) \leq \sigma_i \\ &i, j \in V,\ m = 0, 1, \cdots, m_p - 1 \end{aligned} \tag{32}$$

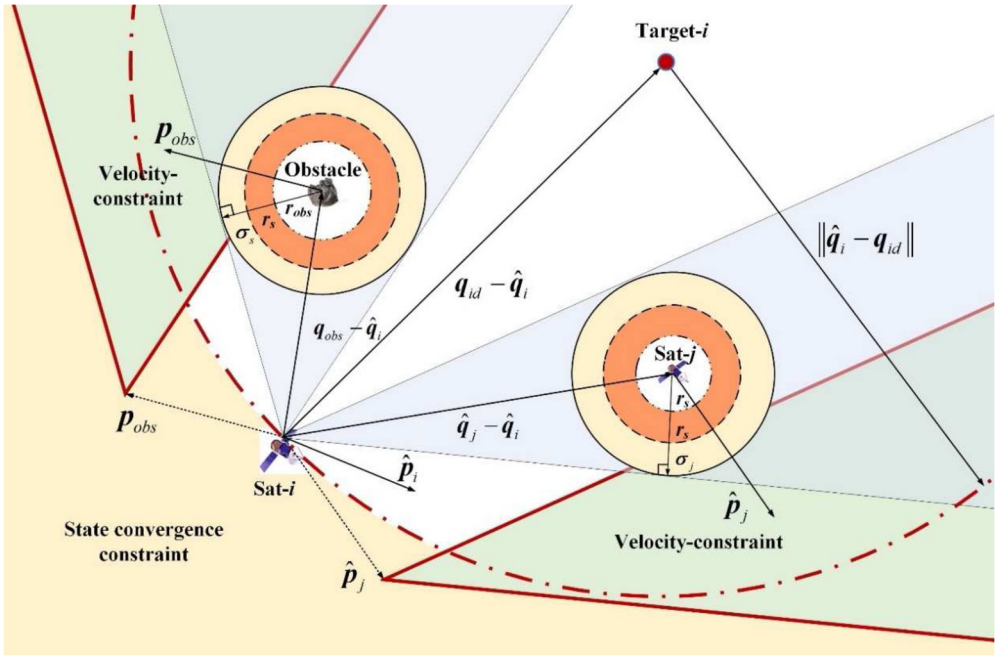

Fig. 4. Terminal velocity constraints of the i-th satellite.

where Ξ_i is the state constraint set, Ξ_{if} is the terminal state constraint set and the $\mathbf{U}_i$ is the constraint set of control force, $\ominus$ denotes the Pontryagin difference, σ_i is a positive constant. $V_i\left(t_k+(m+1)\,\Delta t \mid t_k, \boldsymbol{\zeta}_i, \boldsymbol{\zeta}_{id}\right)=\alpha_i\left\|\tilde{\boldsymbol{q}}_i\left(t_k+m\Delta t \mid t_k\right)-\boldsymbol{q}_{id}\right\|^2$ is the control Lyapunov function. However, it is clear that some constraints are related to the actual trajectory in Eq. (32). Under the action of tube-based auxiliary controller, the position vectors of the actual system and nominal system will satisfy the following inequality

$$\left\|\boldsymbol{q}_i\left(t_k+m\Delta t \mid t_k\right)-\hat{\boldsymbol{q}}_i\left(t_k+m\Delta t \mid t_k\right)\right\| \leq \overline{\boldsymbol{\varepsilon}}_i \tag{33}$$

According to Eq. (33), the conclusion can be obtained that if

$$\left\|\hat{\boldsymbol{q}}_i\left(t_k+m\Delta t \mid t_k\right)-\hat{\boldsymbol{q}}_j\left(t_k+m\Delta t \mid t_k\right)\right\| \geq 2r_s+\overline{\boldsymbol{\varepsilon}}_i+\overline{\boldsymbol{\varepsilon}}_j \tag{34}$$

then the condition of collision avoidance can be satisfied naturally as

$$\left\|\boldsymbol{q}_i\left(t_k+m\Delta t \mid t_k\right)-\boldsymbol{q}_j\left(t_k+m\Delta t \mid t_k\right)\right\| \geq 2r_s \tag{35}$$

In addition, the control force of the actual system is the sum of $\tilde{\boldsymbol{u}}_i$ and auxiliary control $\boldsymbol{\kappa}_i$, and the constraint on the control force need to be modified as well. So, the optimization problem for nominal system can be rewritten as

$$J_i^*\left(\boldsymbol{\zeta}_i^*, \boldsymbol{u}_i^*, t_k\right)=\min_{\tilde{\boldsymbol{u}}_i} J_i\left(t_k, \boldsymbol{\zeta}_i, \boldsymbol{\zeta}_{-i}, \boldsymbol{\zeta}_{id}, \tilde{\boldsymbol{u}}_i, \lambda_i\right)$$

s.t.

$$\begin{aligned}
&\boldsymbol{\zeta}_i\left(t_k+(m+1)\,\Delta t \mid t_k\right)=g\left(\boldsymbol{\zeta}_i\left(t_k+m\Delta t \mid t_k\right), \tilde{\boldsymbol{u}}_i, \Delta t\right)\\
&\boldsymbol{\zeta}_i\left(t_k+m\Delta t \mid t_k\right) \in \Xi_i\\
&\boldsymbol{\zeta}_i\left(t_k+m_p\Delta t \mid t_k\right) \in \Xi_{if}\\
&\tilde{\boldsymbol{u}}_i\left(t_k+m\Delta t \mid t_k\right) \in \mathbf{U}_i\\
&\left\|\hat{\boldsymbol{q}}_i\left(t_k+m\Delta t \mid t_k\right)-\hat{\boldsymbol{q}}_j\left(t_k+m\Delta t \mid t_k\right)\right\| \geq 2r_s+\overline{\boldsymbol{\varepsilon}}_i+\overline{\boldsymbol{\varepsilon}}_j\\
&\left\|\hat{\boldsymbol{q}}_i\left(t_k+m\Delta t \mid t_k\right)-\hat{\boldsymbol{q}}_{obs}\left(t_k+m\Delta t \mid t_k\right)\right\| \geq r_s+r_{obs}+\overline{\boldsymbol{\varepsilon}}_i\\
&V_i\left(t_k+(m+1)\,\Delta t \mid t_k, \boldsymbol{\zeta}_i, \boldsymbol{\zeta}_{id}\right)-V_i\left(t_k+m\Delta t \mid t_k, \boldsymbol{\zeta}_i, \boldsymbol{\zeta}_{id}\right)\\
&\quad \leq -\left(\sigma_i-\lambda_i\left(t_k+m\Delta t \mid t_k\right)\right) V_i\left(t_k+m\Delta t \mid t_k, \boldsymbol{\zeta}_i, \boldsymbol{\zeta}_{id}\right)\\
&\lambda_i\left(t_k+m\Delta t \mid t_k\right) \leq \sigma_i\\
&i,\, j \in V,\ m=0,1,\cdots,m_p-1
\end{aligned} \tag{36}$$

In order to ensure the stability and feasibility of the optimization problem, the design of terminal constraint set Ξ_{if} and terminal controller $\boldsymbol{\rho}_i\left(\boldsymbol{\zeta}_i\left(t_k+m_p\Delta t \mid t_k\right)\right)$ is essential. For the terminal constraint set Ξ_{if}, we employ constraint on the terminal velocity $\hat{\boldsymbol{p}}_i\left(t_k+m_p\Delta t \mid t_k\right)$ which is shown in Fig. 4.

In Fig. 4, $\boldsymbol{p}_{obs}$ is the velocity vector of the space obstacle and the expressions of $\boldsymbol{\sigma}_s$ and $\boldsymbol{\sigma}_j$ are as follows

$$\begin{cases} \boldsymbol{\sigma}_s = \overline{\boldsymbol{\varepsilon}}_i + \left\| \iint_{t_k+m_p\Delta t}^{t_k+(m_p+1)\Delta t} f\left(\tilde{\boldsymbol{q}}_i, \tilde{\boldsymbol{p}}_i, t\right) \mathrm{d}t\mathrm{d}t \right\| \\ \boldsymbol{\sigma}_j = \overline{\boldsymbol{\varepsilon}}_i + \overline{\boldsymbol{\varepsilon}}_j + \left\| \iint_{t_k+m_p\Delta t}^{t_k+(m_p+1)\Delta t} f\left(\tilde{\boldsymbol{q}}_i, \tilde{\boldsymbol{p}}_i, t\right) \mathrm{d}t\mathrm{d}t \right\| \end{cases} \tag{37}$$

where $\left\| \iint_{t_k+m_p\Delta t}^{t_k+(m_p+1)\Delta t} f\left(\tilde{\boldsymbol{q}}_i, \tilde{\boldsymbol{p}}_i, t\right) \mathrm{d}t\mathrm{d}t \right\|$ represents the distance generated by the i-th satellite dynamics in a sample time. And it can be seen that when $\hat{\boldsymbol{p}}_i\left(t_k + m_p\Delta t \mid t_k\right)$ satisfies the condition that the relative velocity between the i-th satellite and obstacle or other satellites is outside the velocity and state convergence constraints, no collision will occur even if the i-th satellite keeps moving to the next sampling time. At the same time, the distance between the i-th satellite and its target will not increase.

Assumption 1. The $\boldsymbol{q}_{obs}$ and $\boldsymbol{p}_{obs}$ of space obstacle can be measured in real time by the satellites in cluster during the process of reconfiguration.

Under the condition of Assumption 1, the terminal constraint set $\boldsymbol{\Xi}_{if}$ of the nominal system can be designed as follows

$$\boldsymbol{\Xi}_{if} = \left\{ \begin{array}{l} \left\| \tilde{\boldsymbol{q}}_i\left(t_k + T_p \mid t_k\right) - \tilde{\boldsymbol{q}}_j\left(t_k + T_p \mid t_k\right) \right\| \geq 2r_s + \boldsymbol{\sigma}_j, \\ \left\| \tilde{\boldsymbol{q}}_i\left(t_k + T_p \mid t_k\right) - \tilde{\boldsymbol{q}}_{obs}\left(t_k + T_p \mid t_k\right) \right\| \geq r_s + r_{obs} + \boldsymbol{\sigma}_s, \\ \left\| \tilde{\boldsymbol{q}}_i\left(t_k + T_p \mid t_k\right) + \iint_{t_k+m_p\Delta t}^{t_k+(m_p+1)\Delta t} f\left(\tilde{\boldsymbol{q}}_i, \tilde{\boldsymbol{p}}_i, t\right) \mathrm{d}t\mathrm{d}t - \tilde{\boldsymbol{q}}_j\left(t_k + T_p \mid t_k\right) - \iint_{t_k+m_p\Delta t}^{t_k+(m_p+1)\Delta t} f\left(\tilde{\boldsymbol{q}}_j, \tilde{\boldsymbol{p}}_j, t\right) \mathrm{d}t\mathrm{d}t \right\| \\ \qquad\qquad \geq 2r_s + \overline{\boldsymbol{\varepsilon}}_i + \overline{\boldsymbol{\varepsilon}}_j, \\ \left\| \tilde{\boldsymbol{q}}_i\left(t_k + T_p \mid t_k\right) + \iint_{t_k+m_p\Delta t}^{t_k+(m_p+1)\Delta t} f\left(\tilde{\boldsymbol{q}}_i, \tilde{\boldsymbol{p}}_i, t\right) \mathrm{d}t\mathrm{d}t - \boldsymbol{q}_{obs}\left(t_k + T_p \mid t_k\right) + \Delta t \cdot \boldsymbol{p}_{obs}\left(t_k + T_p \mid t_k\right) \right\| \geq r_s + r_{obs} + \overline{\boldsymbol{\varepsilon}}_i, \\ \left\| \tilde{\boldsymbol{q}}_i\left(t_k + T_p \mid t_k\right) + \iint_{t_k+m_p\Delta t}^{t_k+(m_p+1)\Delta t} f\left(\tilde{\boldsymbol{q}}_i, \tilde{\boldsymbol{p}}_i, t\right) \mathrm{d}t\mathrm{d}t - \boldsymbol{q}_{id} \right\| \leq \left\| \tilde{\boldsymbol{q}}_i\left(t_k + T_p \mid t_k\right) - \boldsymbol{q}_{id} \right\| \end{array} \right\} \tag{38}$$

The expression of the terminal controller is

$$\boldsymbol{\rho}_i\left(\boldsymbol{\zeta}_i\left(t_k + m_p\Delta t \mid t_k\right)\right) = \boldsymbol{0} \tag{39}$$

According to the Eq. (25) and Eq. (39), it can be found that the i-th satellite will keep moving at the velocity of $\tilde{\boldsymbol{p}}_i\left(t_k + m_p\Delta t \mid t_k\right)$ under the action of $\boldsymbol{\rho}_i\left(\boldsymbol{\zeta}_i\left(t_k + m_p\Delta t \mid t_k\right)\right)$.

Lemma 2 *([32]). For a general discrete-time system $x(k+1) = f(x(k))$, where $x \in \mathbf{X} \subseteq \mathbf{R}^n$, $f : \mathbf{R}^n \to \mathbf{R}^n$, $k \in \mathbf{Z}_+$ and $f(0) = 0$, the function $V(x)$ is called a control Lyapunov function if the following holds:*

1) *There exist two K_∞-functions μ_1 and μ_2 such that*

$$\mu_1(\|x\|) \leq V(x) \leq \mu_2(\|x\|) \tag{40}$$

2) *There exists a K_∞-function μ_3 such that*

$$V(f(x)) - V(x) \leq -\mu_3(\|x\|) \tag{41}$$

Let $V(x)$ be the Lyapunov function of $x(k+1) = f(x(k))$, the origin is an asymptotically stable equilibrium in $\mathbf{X}$.

Assumption 2. The targets of the i-th satellite and the j-th satellite and the position vector of the obstacle satisfy the following relation

$$\begin{cases} \left\| \boldsymbol{q}_{id} - \boldsymbol{q}_{jd} \right\| \geq 2r_s + \overline{\boldsymbol{\varepsilon}}_i + \overline{\boldsymbol{\varepsilon}}_j \\ \left\| \boldsymbol{q}_{id} - \boldsymbol{q}_{obs} \right\| \geq r_s + r_{obs} + \overline{\boldsymbol{\varepsilon}}_i \end{cases} \tag{42}$$

Assumption 3. There exist positive constants μ_1, μ_2, c_1 and c_2 such that

$$\mu_1 \left\| \tilde{\boldsymbol{q}}_i\left(t_k + m\Delta t \mid t_k\right) - \tilde{\boldsymbol{q}}_{id} \right\|^{c_1} \leq J_i\left(t_k, \boldsymbol{\zeta}_i, \boldsymbol{\zeta}_{-i}, \boldsymbol{\zeta}_{id}, \tilde{\boldsymbol{u}}_i, \lambda_i\right) \leq \mu_1 \left\| \tilde{\boldsymbol{q}}_i\left(t_k + m\Delta t \mid t_k\right) - \tilde{\boldsymbol{q}}_{id} \right\|^{c_2} \tag{43}$$

Assumption 4. There exist positive constants μ_3 and T_r such that when the prediction horizon $T_p \geq T_r$, $\sigma_i > \lambda_i$ in at least one sampling time during the prediction process and make $\sum_{m=0}^{m_p-1}\left(\sigma_i - \lambda_i\left(t_k + m\Delta t \mid t_k\right)\right) \geq \mu_3$.

Remark 1. Assumption 2 guarantees that the position of the target point and the obstacle satisfies the state constraints of the nominal system which will not cause the controller to have no solution at the final moment. In practice, the states and control forces of the nominal system are bounded. So, Assumption 3 is reasonable. Assumption 4 ensures that there is at least one moment in each prediction horizon that the i-th satellite is moving close to the target point. It can also be satisfied as long as the satellites and obstacles in space are not particularly crowded.

Theorem 2. *Suppose that the optimization problem described by Eq. (36) has an initial feasible solution at t_k and Assumption 1-3 is satisfied. Choose the prediction horizon $T_p \geq T_r$, then the optimization problem will be feasible at any time $t_k + n\Delta t$, $n \in \mathbf{Z}_+$. The nominal system of Eq. (25) will be asymptotically stable. That is $\|\tilde{\boldsymbol{q}}_i - \boldsymbol{q}_{id}\| \to 0$ when $n \to \infty$. The actual system will be will converge to a bounded range around the equilibrium point which can be expressed as $\|\boldsymbol{q}_i - \boldsymbol{q}_{id}\| \leq \overline{\boldsymbol{\varepsilon}}_i$.*

Proof. Suppose that the optimal control sequence and optimal trajectory at t_k can be expressed as $\boldsymbol{u}_i^*(t_k + m\Delta t \mid t_k)$ and $\boldsymbol{\zeta}_i^*(t_k + m\Delta t \mid t_k)$ where $m = 0, 1, \cdots, m_p - 1$. Then calculate one step further using terminal controller and we will get the feasible control sequence $\hat{\boldsymbol{u}}_i(t_k + m\Delta t \mid t_{k+1})$ and feasible trajectory $\hat{\boldsymbol{\zeta}}_i(t_k + m\Delta t \mid t_{k+1})$ during $m = 0, 1, \cdots, m_p - 1$.

According to the Assumption 1, there exist two K_∞-functions μ_1 and μ_2 making the optimal states cost function $J_i^{H^*}(t_k, \boldsymbol{\zeta}_i^*, \boldsymbol{\zeta}_{-i}, \boldsymbol{\zeta}_{id}, \boldsymbol{u}_i^*)$ of the i-th satellite satisfy the following condition

$$\mu_1\left(\left\|\Delta\boldsymbol{\zeta}_i^*\right\|\right) \leq J_i^{H^*}\left(t_k, \boldsymbol{\zeta}_i^*, \boldsymbol{\zeta}_{-i}, \boldsymbol{\zeta}_{id}, \boldsymbol{u}_i^*\right) \leq \mu_2\left(\left\|\Delta\boldsymbol{\zeta}_i^*\right\|\right) \tag{44}$$

where $\left\|\Delta\boldsymbol{\zeta}_i^*\right\| = \sum_{m=0}^{m_p-1} \alpha_i \left\|\tilde{\boldsymbol{q}}_i(t_k + m\Delta t \mid t_k) - \boldsymbol{q}_{id}\right\|$. Define $\hat{J}_i^H\left(t_{k+1}, \hat{\boldsymbol{\zeta}}_i, \boldsymbol{\zeta}_{-i}, \boldsymbol{\zeta}_{id}, \hat{\boldsymbol{u}}_i\right)$ is the feasible states cost function and it can be obtained that

$$\begin{aligned}
&\hat{J}_i^H\left(t_{k+1}, \hat{\boldsymbol{\zeta}}_i, \boldsymbol{\zeta}_{-i}, \boldsymbol{\zeta}_{id}, \hat{\boldsymbol{u}}_i\right) - J_i^{H^*}\left(t_k, \boldsymbol{\zeta}_i^*, \boldsymbol{\zeta}_{-i}, \boldsymbol{\zeta}_{id}, \boldsymbol{u}_i^*\right) \\
&= \sum_{m=0}^{m_p-1} \alpha_i \left\|\tilde{\boldsymbol{q}}_i\left(t_{k+1} + m\Delta t \mid t_{k+1}\right) - \boldsymbol{q}_{id}\right\|^2 + \beta_i \left\|\tilde{\boldsymbol{u}}_i\left(t_{k+1} + m\Delta t \mid t_{k+1}\right)\right\|^2 \\
&\quad - \sum_{m=0}^{m_p-1} \alpha_i \left\|\boldsymbol{q}_i^*(t_k + m\Delta t \mid t_k) - \boldsymbol{q}_{id}\right\|^2 + \beta_i \left\|\boldsymbol{u}_i^*(t_k + m\Delta t \mid t_k)\right\|^2
\end{aligned} \tag{45}$$

Since $\hat{J}_i^H\left(t_k, \hat{\boldsymbol{\zeta}}_i, \boldsymbol{\zeta}_{-i}, \boldsymbol{\zeta}_{id}, \hat{\boldsymbol{u}}_i\right) = J_i^{H^*}\left(t_k, \boldsymbol{\zeta}_i^*, \boldsymbol{\zeta}_{-i}, \boldsymbol{\zeta}_{id}, \boldsymbol{u}_i^*\right)$, the Eq. (45) can be recast as

$$\begin{aligned}
&\hat{J}_i^H\left(t_{k+1}, \hat{\boldsymbol{\zeta}}_i, \boldsymbol{\zeta}_{-i}, \boldsymbol{\zeta}_{id}, \hat{\boldsymbol{u}}_i\right) - J_i^{H^*}\left(t_k, \boldsymbol{\zeta}_i^*, \boldsymbol{\zeta}_{-i}, \boldsymbol{\zeta}_{id}, \boldsymbol{u}_i^*\right) \\
&= \sum_{m=0}^{m_{p-1}} \left(V_i\left(t_{k+1} + m\Delta t \mid t_k, \boldsymbol{\zeta}_i, \boldsymbol{\zeta}_{id}\right) - V_i\left(t_k + m\Delta t \mid t_k, \boldsymbol{\zeta}_i^*, \boldsymbol{\zeta}_{id}\right)\right) \\
&\quad + \beta_i \left\|\boldsymbol{\rho}_i\left(\boldsymbol{\zeta}_i(t_k + m\Delta t \mid t_k)\right)\right\|^2 - \beta_i \left\|\boldsymbol{u}_i^*(t_k \mid t_k)\right\|^2
\end{aligned} \tag{46}$$

When $t \in \left[t_k + m_p\Delta t, t_{k+1} + m_p\Delta t\right]$

$$\boldsymbol{\rho}_i\left(\boldsymbol{\zeta}_i\left(t_k + m_p\Delta t \mid t_k\right)\right) = \mathbf{0} \tag{47}$$

Then, Eq. (46) can be rewritten as

$$\begin{aligned}
&\hat{J}_i^H\left(t_{k+1}, \hat{\boldsymbol{\zeta}}_i, \boldsymbol{\zeta}_{-i}, \boldsymbol{\zeta}_{id}, \hat{\boldsymbol{u}}_i\right) - J_i^{H^*}\left(t_k, \boldsymbol{\zeta}_i^*, \boldsymbol{\zeta}_{-i}, \boldsymbol{\zeta}_{id}, \boldsymbol{u}_i^*\right) \\
&\leq \sum_{m=0}^{m_{p-1}} \left(-\left(\sigma_i - \lambda_i(t_k + m\Delta t \mid t_k)\right) V_i\left(t_k + m\Delta t \mid t_k, \boldsymbol{\zeta}_i, \boldsymbol{\zeta}_{id}\right)\right) - \beta_i \left\|\boldsymbol{u}_i^*(t_k \mid t_k)\right\|^2
\end{aligned} \tag{48}$$

According to Assumption 3 it has

$$\begin{aligned}
&\hat{J}_i^H\left(t_{k+1}, \hat{\boldsymbol{\zeta}}_i, \boldsymbol{\zeta}_{-i}, \boldsymbol{\zeta}_{id}, \hat{\boldsymbol{u}}_i\right) - J_i^{H^*}\left(t_k, \boldsymbol{\zeta}_i^*, \boldsymbol{\zeta}_{-i}, \boldsymbol{\zeta}_{id}, \boldsymbol{u}_i^*\right) \\
&\leq -\mu_3 \sum_{m=0}^{m_{p-1}} \left(V_i\left(t_k + m\Delta t \mid t_k, \boldsymbol{\zeta}_i, \boldsymbol{\zeta}_{id}\right)\right)
\end{aligned} \tag{49}$$

Thus, it can infer that

$$J_i^{H^*}\left(t_{k+1}, \boldsymbol{\zeta}_i^*, \boldsymbol{\zeta}_{-i}, \boldsymbol{\zeta}_{id}, \boldsymbol{u}_i^*\right) \leq \hat{J}_i^H\left(t_{k+1}, \hat{\boldsymbol{\zeta}}_i, \boldsymbol{\zeta}_{-i}, \boldsymbol{\zeta}_{id}, \hat{\boldsymbol{u}}_i\right) < J_i^{H^*}\left(t_k, \boldsymbol{\zeta}_i^*, \boldsymbol{\zeta}_{-i}, \boldsymbol{\zeta}_{id}, \boldsymbol{u}_i^*\right) \tag{50}$$

According to the condition of in Lemma 2, $J_i^{H^*}\left(t_{k+1}, \boldsymbol{\zeta}_i^*, \boldsymbol{\zeta}_{-i}, \boldsymbol{\zeta}_{id}, \boldsymbol{u}_i^*\right)$ will converge to 0 under the action of the optimal control sequence. Thus, the closed loop stability of the nominal system is proved. □

Table 1
Time complexity comparison of allocation algorithms.

Allocation algorithm	Time complexity
Exhaustive method	$O(n \times n!)$
Backtrack algorithm	$O(n^n)$
Branch and bound algorithm	$O(n^n)$
Hungarian algorithm	$O(n^3)$

Moreover, if the states of i-th satellite satisfied the terminal constraint set $\boldsymbol{\Xi}_{if}$ at $t_k + T_p$, terminal controller $\boldsymbol{\rho}_i\left(\boldsymbol{\zeta}_i\left(t_k + m_p\Delta t \mid t_k\right)\right) = \mathbf{0}$ can make it continue to move at the speed of time $t_k + T_p$. According to Eq. (38), all constraints can still be satisfied. Therefore, the feasibility of the controller can be guaranteed.

In summary, the rolling optimization process of the RDMPC controller is as follows:

Off-line stage: First, give the spatial position vectors of all target points according to the task requirements. Then, set the parameters α_i, β_i and γ_i in the cost function for each satellite in the cluster and determine the constraint parameters $\boldsymbol{\Xi}_i$, $\boldsymbol{\Xi}_{if}$, $\mathbf{U}_i$, r_s, r_{obs} and σ_i in optimization problem Eq. (36). Moreover, according to the initial states of the satellites, compute the initial adjacency matrix A of the satellite cluster network. Finally, give the gain coefficients k_1 and k_2 of the Tube-based auxiliary controller $\boldsymbol{\kappa}_i$.

On-line stage: At the initialization time t_0, the Hungarian algorithm is adopted to match the satellites with the target points one by one according to the initial position of the satellites. Then, give the initial optimal control sequence $\boldsymbol{u}_i^*\left(t_0 + m\Delta t \mid t_0\right)$ and the initial optimal states $\boldsymbol{\zeta}_i^*\left(t_0 + m\Delta t \mid t_0\right)$ for $m = 0, 1, \ldots, m_p - 1$. And the following procedure is

Step 1. Transmit the nominal predicted states $\hat{\boldsymbol{\zeta}}_i\left(t_k + m\Delta t \mid t_k\right)$ of the i-th satellite to its neighbor satellites according to the adjacency matrix A of the cluster satellites in the current communication network, where $k \geq 0$.

Step 2. Solve the optimization problem Eq. (36) of the i-th satellite using the predicted states of the neighbor satellites and the motion information of the space obstacles. Then the optimized control sequence $\boldsymbol{u}_i^*\left(t_k + m\Delta t \mid t_k\right)$ can be obtained.

Step 3. Apply the first term $\boldsymbol{u}_i^*\left(t_k \mid t_k\right)$ in the optimal control sequence $\boldsymbol{u}_i^*\left(t_k + m\Delta t \mid t_k\right)$ as the control force to the nominal system and gets the states $\hat{\boldsymbol{\zeta}}_i(t)$ of the nominal system in the interval $[t_k, t_{k+1}]$. Compute the auxiliary control law $\boldsymbol{\kappa}_i$ and superimpose it with $\boldsymbol{u}_i^*\left(t_k \mid t_k\right)$ to act on the actual system. Then obtains the states $\boldsymbol{\zeta}_i\left(t_{k+1} \mid t_{k+1}\right)$ of the actual system.

Step 4. Update the targets allocation and adjacency matrix A of the satellite cluster. Calculate the predicted states $\hat{\boldsymbol{\zeta}}_i\left(t_{k+1} + m\Delta t \mid t_{k+1}\right)$ of the i-th satellite by applying the optimized control sequence $\boldsymbol{u}_i^*\left(t_k + m\Delta t \mid t_k\right)$ to the nominal system. Then transmit the predicted state of the i-th satellite states to its neighbor satellites and return to Step 2.

3.3. Optimization of target point allocation based on Hungary algorithm

In practice, satellite cluster usually consists of several small satellites with the same functional modules. In this way, assigning any satellite to the certain target point would meet the mission requirements. However, the distances between satellites in cluster and each target point are different, thus allocating different target points to each satellite in a reasonable manner can reduce the total fuel consumption and the action of collision avoidance. Since satellites and target points are assigned one to one, the Hungarian optimization algorithm is a good choice to solve this problem.

The Hungarian algorithm is a combinatorial optimization algorithm for solving task assignment problems in polynomial time which was proposed by Harold Kuhn in 1965 [31]. For the assignment problem between satellites and target points, the key is to assign a certain target to each satellite so as to minimize the total cost. Besides the Hungarian algorithm, there are many ways to deal with the target assignment problem. But among these methods, the Hungarian algorithm has the least time complexity, as shown in Table 1.

It can be seen from Table 1 that with the number of allocated targets increases, the time complexity corresponding to the Hungarian algorithm has more advantages than other allocation algorithms. Therefore, the classical Hungarian algorithm is adopted to achieve the optimal allocation of targets in this section. According to the optimization principle of Hungarian algorithm and the cost function of distributed MPC controller mentioned above, we can define the cost matrix C as $C_{ij} = \alpha_i \left\| \boldsymbol{q}_i - \boldsymbol{q}_{id} \right\|^2$, where $i, j = 1, 2, \cdots, n$. C_{ij} denotes the cost of i-th satellite to the j-th target point. Then, the specific steps are as follows:

Step 1. Calculate the cost matrix C using the current state information of each satellite and target. In the cost matrix, rows correspond to satellites and columns to target points. Go to Step 2.

Step 2. Search the smallest element in each row of cost matrix C and subtract it from all elements which in the same row. Go to Step 3.

Step 3. Search the smallest element in each column of cost matrix C and subtract it from all elements which in the same column. Go to Step 4.

Step 4. Cover all zero elements of cost matrix C with the fewest horizontal or vertical lines and count the number of lines as l. Go to Step 5.

Step 5. Determine the value of l and n, and it can get two results: (1) If $l < n$, it indicates that the optimization result has not been obtained. Go to Step 6. (2) If $l = n$, it indicates that the assignment optimization is complete. The position of zero elements in cost matrix C represents the result of assignment optimization.

Table 2
The initial position vectors of the 10 satellites in Case 1.

Satellite	Initial position vector (m)	Satellite	Initial position vector (m)
1	$q_1(0) = [946.1\ 1025.3\ 666.3]^{\mathrm{T}}$	6	$q_6(0) = [803.4\ 707.3\ 1085.3]^{\mathrm{T}}$
2	$q_2(0) = [628.1\ 973.3\ 625.6]^{\mathrm{T}}$	7	$q_7(0) = [669.3\ 1028.2\ 944.6]^{\mathrm{T}}$
3	$q_3(0) = [801.3\ 501.1\ 825.7]^{\mathrm{T}}$	8	$q_8(0) = [937.3\ 727.1\ 543.4]^{\mathrm{T}}$
4	$q_4(0) = [525.5\ 734.1\ 901.6]^{\mathrm{T}}$	9	$q_9(0) = [632.3\ 656.5\ 596.7]^{\mathrm{T}}$
5	$q_5(0) = [981.6\ 960.1\ 977.1]^{\mathrm{T}}$	10	$q_{10}(0) = [1075.9\ 687.1\ 833.6]^{\mathrm{T}}$

Table 3
The initial position vectors of the 10 satellites in Case 2.

Satellite	Initial position vector (m)	Satellite	Initial position vector (m)
1	$q_1(0) = [490.6\ 560.7\ 805.9]^{\mathrm{T}}$	6	$q_6(0) = [1619.1\ 900.2\ 1311.2]^{\mathrm{T}}$
2	$q_2(0) = [856.3\ 1070.5\ 318.5]^{\mathrm{T}}$	7	$q_7(0) = [424.5\ 1382.5\ 888.1]^{\mathrm{T}}$
3	$q_3(0) = [512.7\ 969.1\ 1501.6]^{\mathrm{T}}$	8	$q_8(0) = [1566.1\ 1163.7\ 622.3]^{\mathrm{T}}$
4	$q_4(0) = [1262.7\ 442.7\ 667.7]^{\mathrm{T}}$	9	$q_9(0) = [1112.2\ 1682.3\ 891.4]^{\mathrm{T}}$
5	$q_5(0) = [1033.4\ 439.1\ 1417.3]^{\mathrm{T}}$	10	$q_{10}(0) = [1119.9\ 1385.1\ 1572.2]^{\mathrm{T}}$

Table 4
The target position vectors of the 10 satellites in the LVLH frame.

Satellite	Target position vector (m)	Satellite	Target position vector (m)
1	$q_{1d} = [-189.9\ -11.8\ -433.5]^{\mathrm{T}}$	6	$q_{6d} = [-393.8\ -403.2\ -94.4]^{\mathrm{T}}$
2	$q_{2d} = [-118.7\ 85.5\ -156.7]^{\mathrm{T}}$	7	$q_{7d} = [-476.1\ -83.1\ -189.2]^{\mathrm{T}}$
3	$q_{3d} = [-103.4\ -470.2\ -112.5]^{\mathrm{T}}$	8	$q_{8d} = [-100.3\ -343.3\ -443.9]^{\mathrm{T}}$
4	$q_{4d} = [-310.7\ -112.9\ 64.8]^{\mathrm{T}}$	9	$q_{9d} = [-394.8\ -292.6\ -408.4]^{\mathrm{T}}$
5	$q_{5d} = [-16.1\ -174.3\ 35.5]^{\mathrm{T}}$	10	$q_{10d} = [94.2\ -235.2\ -247.2]^{\mathrm{T}}$

Step 6. Find the smallest element which is not covered by any line. Subtract this element from each row uncovered by lines and add it to each column covered by lines. Return to Step 4.

In this way, we can get the target points assignment optimization of the satellites cluster at any moment. Because the distributed MPC controller computes the control sequence through rolling optimization, we can optimize the target assignment not only at the beginning of the task, but also during the process. It is worth noting that if the target assignment optimization calculation is carried out at each step of the control, it will cause a large computational burden and may get repeated optimization results. Although this optimizing strategy does not guarantee the minimization of fuel, it can reduce trajectory crossing to some extent which is beneficial to collision avoidance of satellites. Therefore, it makes sense to optimize target assignment.

4. Numerical simulations

In this section, several numerical simulations of the RDMPC for satellite cluster reconfiguration are performed. Suppose that the satellite cluster contains 10 follower satellites and the target points are evenly distributed on the space sphere centered on the target spacecraft.

The maximum communication distance between satellites $r_c = 1000$ m and $N_a = 4$. In order to ensure that no collision occurs during the reconfiguration process of satellite cluster, the safe distance between each satellite is set as $r_s = 100$ m and the safe distance from space obstacle is set as $r_o = 300$ m. Moreover, assume that the mass of each satellite in cluster is 50 kg and the amplitude of thruster is constrained by $T_{\max} = 1$ N. The uncertain disturbance is considered as $\boldsymbol{w}_i = \overline{\boldsymbol{w}}_i\,[\sin(0.02t + \pi/3)\ \ \sin(0.02t - 2\pi/3)\ \ \sin(0.02t + \pi/2)]^{\mathrm{T}}$, where $\overline{\boldsymbol{w}}_i = 0.1$.

4.1. Numerical simulations under different initial configurations of cluster

In this section, the reconfiguration control of the satellite cluster will be carried out in two different initial configurations. In the first case, the initial configuration of the satellites is concentrated and the initial position vectors in the LVLH frame are shown in Table 2. For the second case, the initial configuration of the satellites is dispersed and the initial position vectors in the LVLH frame are shown in Table 3. Moreover, consider that the satellites in the cluster have the same initial velocity and $p_i(0) = [0\ 0\ 0]^{\mathrm{T}}$, $i = 1, 2, \cdots, 10$.

In the LVLH frame, the target position vectors of the cluster satellites are shown in Table 4. The position vector of the target spacecraft is $\boldsymbol{q}_r = [-200\ -200\ -200]^{\mathrm{T}}$. The initial position vector of the space obstacle is $\boldsymbol{q}_o(t_0) = [600\ 0\ 0]^{\mathrm{T}}$ and the velocity of it is $\boldsymbol{p}_o(t) = [-0.4\ 0.4\ 0.4]^{\mathrm{T}}$.

Assume the parameters of the auxiliary controller can be designed as $k_1 = 2$ and $k_2 = 4$. The parameters of the RDMPC controller are that $\alpha_i = 1$, $\beta_i = 200$, $\gamma_i = 500$, $\sigma_i = 0.2$. At the same time, the predictive horizon $T_p = 50$ s and the sampling time $\Delta t = 5$ s.

Under the action of the RDMPC controller, the trajectories of the satellites in Case 1 and Case 2 are shown as Fig. 5 and Fig. 6.

It can be seen in Fig. 5 and Fig. 6 that the predictive states and actual states can be converged on the desired target points finally. During the entire movement, the actual trajectories are the same as the nominal trajectories basically. In addition, the spheres in the figure represent the safety range of the target spacecraft and space obstacle and the satellites in cluster have obvious obstacle avoidance behaviors. However, the initial configuration of the satellites is more dispersed in Case 2, so the collision avoidance action of the satellites is greatly reduced. That is the main difference between Case 1 and Case 2.

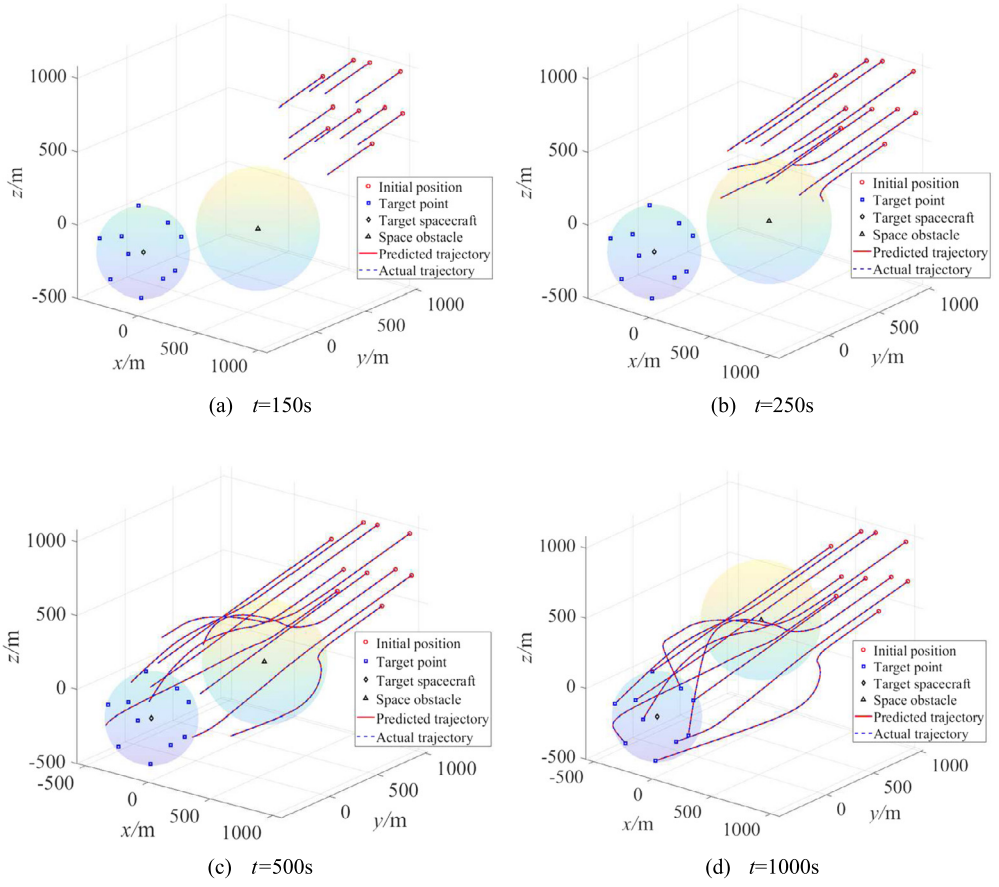

Fig. 5. The trajectories of the satellites under RDMPC controller in Case 1.

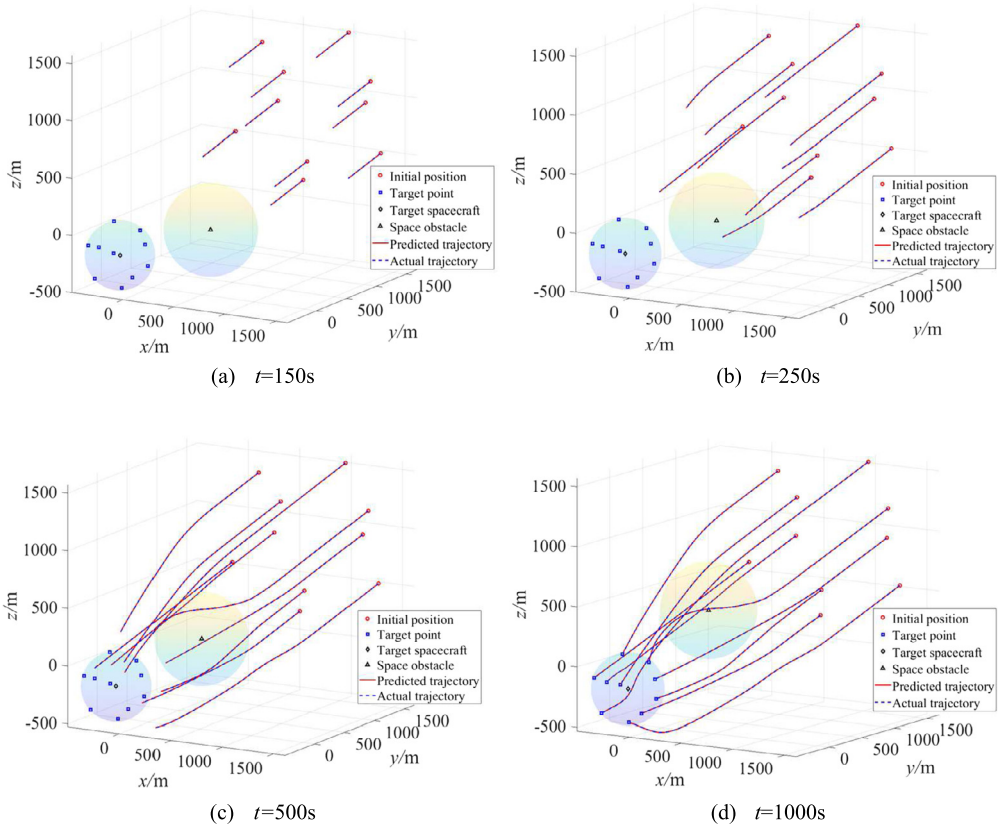

Fig. 6. The trajectories of the satellites under RDMPC controller in Case 2.

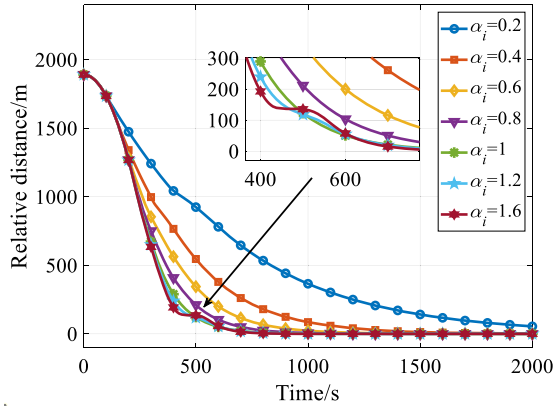

Fig. 7. The relative distance between Sat 1 and target point under different α_i.

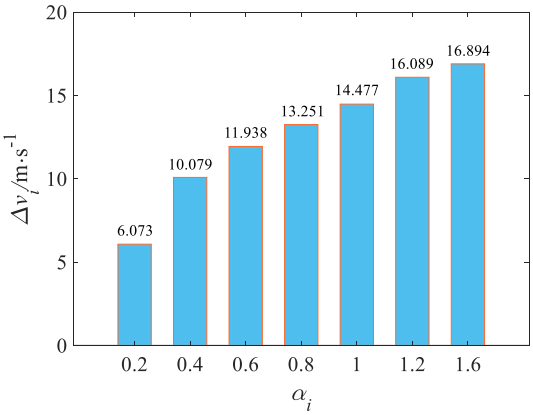

Fig. 8. The fuel consumption of Sat 1 under different α_i.

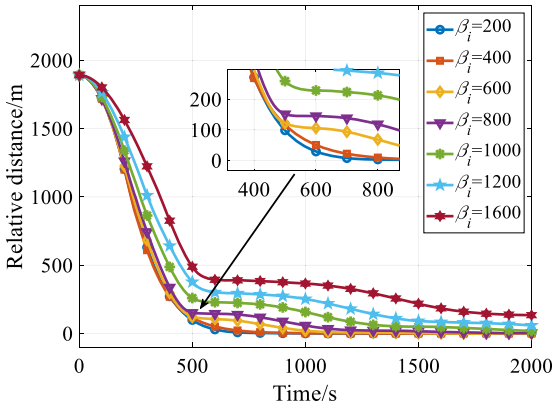

Fig. 9. The relative distance between Sat 1 and target point under different β_i.

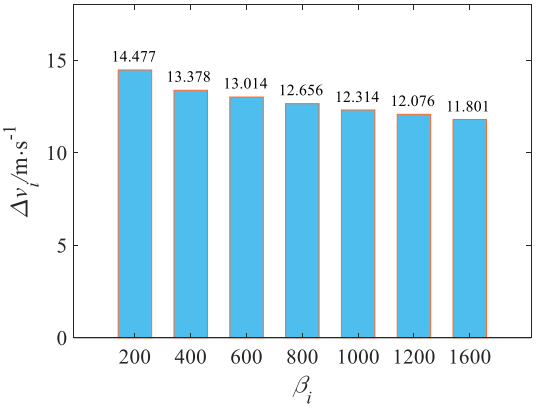

Fig. 10. The fuel consumption of Sat 1 under different β_i.

4.2. Numerical simulations under different controller parameters

In this section, the target points and the initial position vectors of the satellites in cluster are set as the same as Case 1 in Section 4.1. The numerical simulation takes Sat 1 as an example to verify the different control effects of the RDMPC controller and the auxiliary controller under different parameters.

For the RDMPC controller, α_i and γ_i affect the convergence rate of the nominal system and β_i affects the fuel consumption of the satellites in cluster. Firstly, under the condition that $\beta_i = 200$, $\gamma_i = 500$ and α_i takes different values, the relative distance between Sat 1 and target point is shown in Fig. 7 and the fuel consumption of Sat 1 during the movement is shown in Fig. 8.

It can be seen from Fig. 7 that the convergence of Sat 1 increases with the increase of the value of α_i. But due to the upper limit of the thrust amplitude of the thruster and the obstacle avoidance action of the satellite, the convergence rate is not greatly affected by α_i when $\alpha_i \geq 1$. And in Fig. 8, the fuel consumption of Sat 1 increases with α_i.

Then, under the condition that $\alpha_i = 1$, $\gamma_i = 500$ and β_i takes different values, the relative distance between Sat 1 and target point is shown in Fig. 9 and the fuel consumption of Sat 1 during the movement is shown in Fig. 10.

In Fig. 9 and Fig. 10, though the fuel consumption of Sat 1 decreases with the increase of β_i, the speed of satellite convergence is greatly reduced. This is because when the value of β_i is large, the RDMPC controller prioritizes fuel optimization.

Moreover, γ_i also affects the convergence of the nominal system. Under the condition that $\alpha_i = 1$, $\beta_i = 200$ and r_i takes different values, the value of slack variable of Sat 1 is shown in Fig. 11 and the fuel consumption is shown in Fig. 12.

According to Eq. (32), $\sigma_i - \lambda_i$ represents the convergence rate of the nominal system. It can be seen in Fig. 11 and Fig. 12 that λ_i is rapidly reduced under the action of the controller to achieve the rapid convergence of the system when the Sat 1 doesn't perform collision avoidance action. But in the process of collision avoidance, the value of λ_i will give priority to meet the constraints of collision avoidance. With the increase of γ_i, the value of λ_i decreases, and the fuel consumption increases slightly. However, since the thruster amplitude has an upper limit, even if the value of λ_i is large at the beginning of the movement, the convergence rate cannot be increased. Therefore, the main role of λ_i is to quickly restore the convergence rate after the action of obstacle avoidance.

For the auxiliary controller, k_{i1} and k_{i2} determine the value of $\overline{\boldsymbol{\varepsilon}}_i$. According to the condition of Theorem 1, set of parameters is $k_{i2} = 4$ and k_{i1} takes different values. Then, the distance error between actual system and nominal system of Sat 1 is shown in Fig. 13. After simulation verification, the control force curves generated by the auxiliary controller are almost the same in each case, so taking $k_{i1} = 2$ and $k_{i2} = 4$ as examples, the control force curves in three coordinate axes are shown in Fig. 14.

In Fig. 13, the maximum value of the distance error between the actual system and the nominal system decreases gradually when the controller parameter k_{i1} increases. Moreover, the distance error satisfies Eq. (15) mentioned in Theorem 1. Therefore, the parameters of the auxiliary controller can be determined according to the tracking accuracy required for the space mission. It is worth noting in

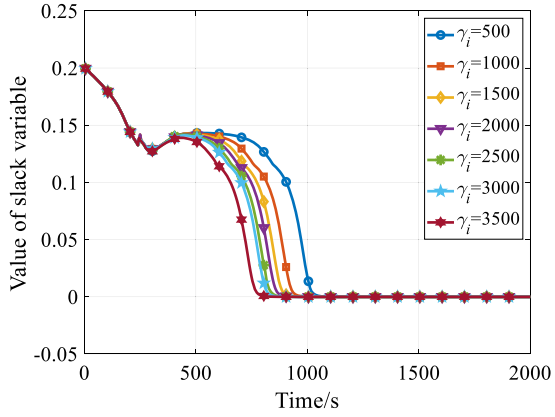

Fig. 11. The value of slack variable of Sat 1 under different γ_i.

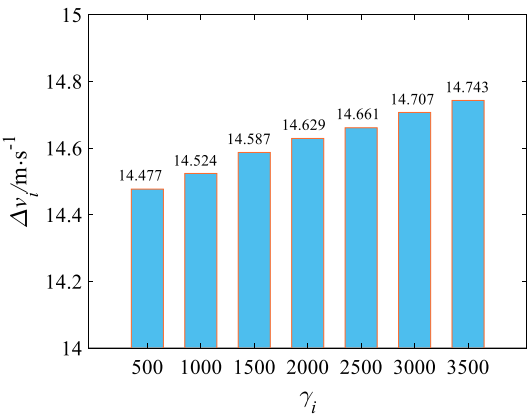

Fig. 12. The fuel consumption of Sat 1 under different γ_i.

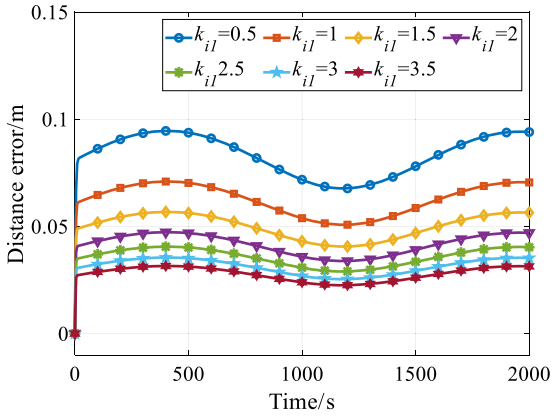

Fig. 13. The distance error between actual system and nominal system of Sat 1 under different k_{i1}.

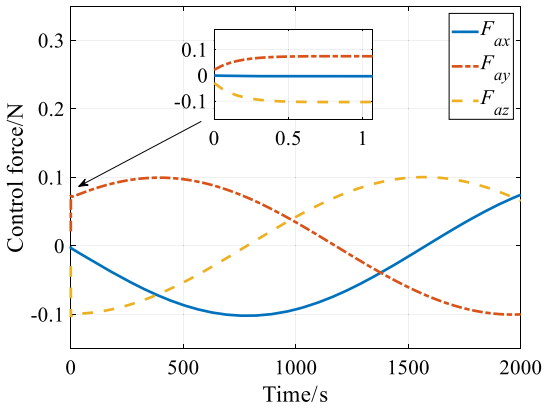

Fig. 14. The control force curves in three coordinate axes of auxiliary controller of Sat 1.

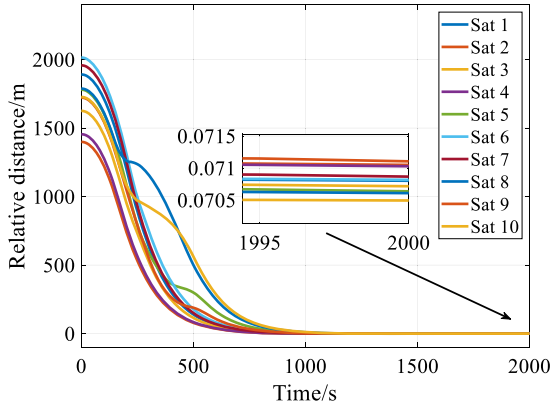

Fig. 15. The distance errors between satellites and targets under RDMPC controller. (For interpretation of the colors in the figures, the reader is referred to the web version of this article.)

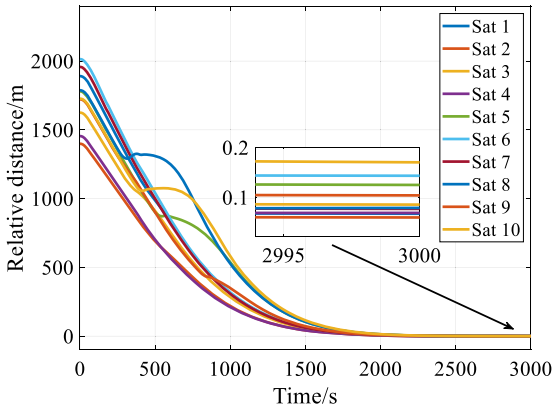

Fig. 16. The distance errors between satellites and targets under artificial potential field controller.

Fig. 14 that since the initial states of the actual system and the nominal system are the same, the auxiliary controller can compensate the uncertain disturbance in a very short time.

4.3. Comparative simulations with artificial potential field method

In this section, the comparative simulations between the artificial potential field method in Ref. [33] and the proposed control strategy in this paper are carried out. Firstly, let the conditions for satellite cluster reconfiguration are the same as Case 1 in Section 4.1. Then, some control effects during the reconfiguration process are compared under the action of two different controllers.

For the target points tracking, the distance errors of the satellites in cluster under the action of the two controllers are shown in Fig. 15 and Fig. 16.

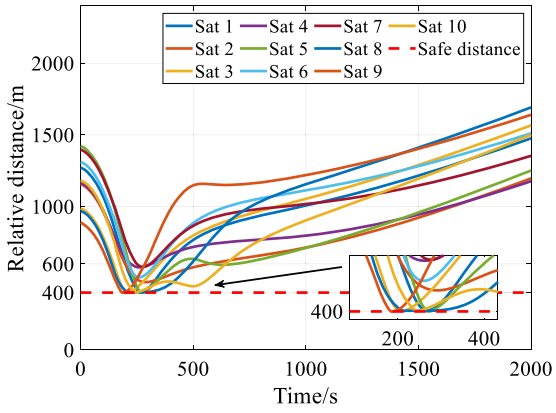

Fig. 17. The distance errors between satellites and space obstacle under RDMPC controller.

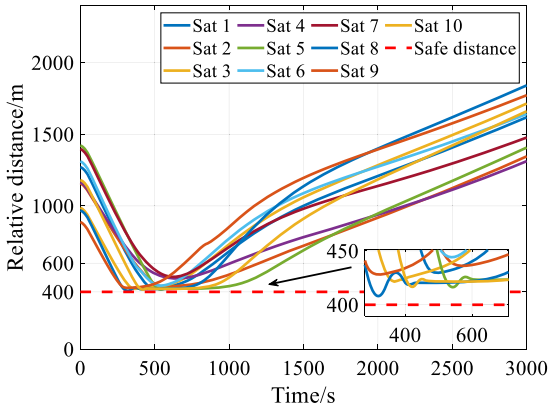

Fig. 18. The distance errors between satellites and space obstacle under artificial potential field controller.

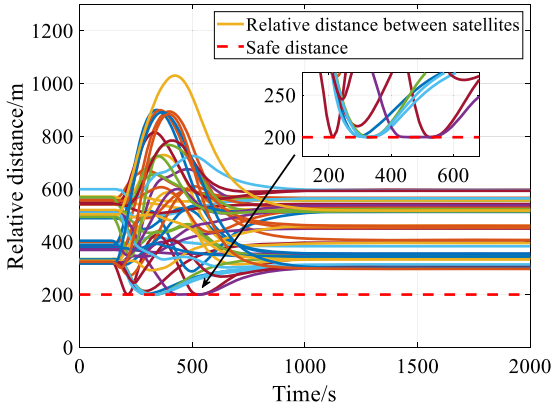

Fig. 19. The distance errors between satellites in cluster under RDMPC controller.

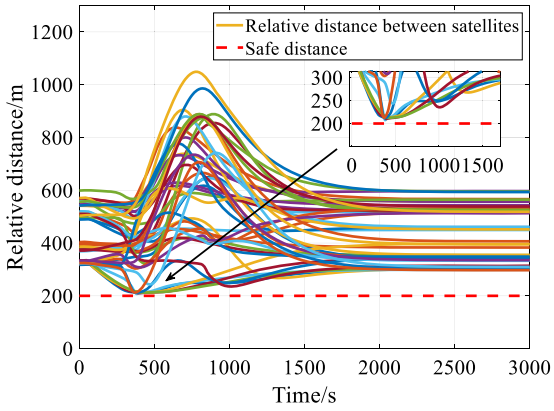

Fig. 20. The distance errors between satellites in cluster under artificial potential field controller.

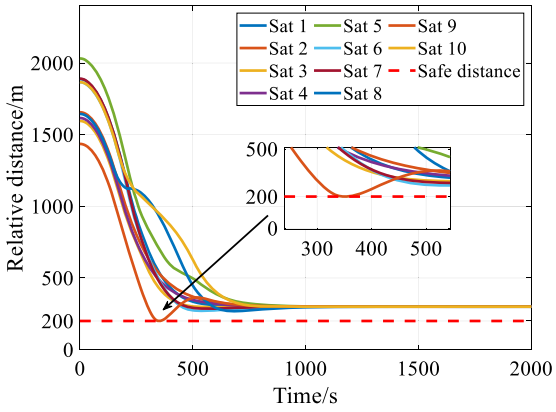

Fig. 21. The distance errors between satellites and target spacecraft under RDMPC controller.

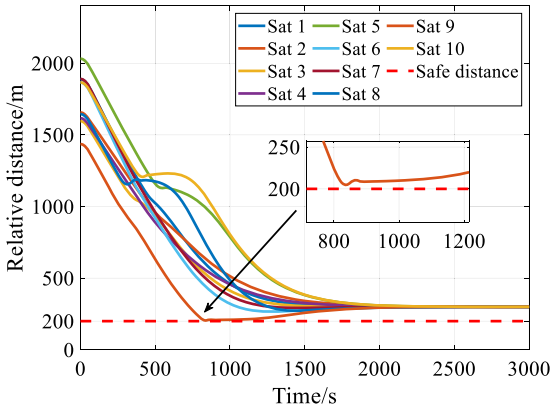

Fig. 22. The distance errors between satellites and target spacecraft under artificial potential field controller.

In Fig. 15, the relative distances between satellites and targets decrease monotonically which means the terminal constraints of the RDMPC controller are satisfied. The convergence time of the distributed RDMPC controller is 1000 s, while the control accuracy is 0.071 m. Comparing Fig. 15 and Fig. 16, the convergence rate of the satellite is faster under the action of the RDMPC controller and the convergence accuracy is higher. This is because the thruster amplitude of each satellite has an upper limit. In this way, in the artificial potential field method controller, the parameters of the attractive potential field cannot be set too large. Otherwise, the collision avoidance of the cluster may not be guaranteed by the repulsive potential function.

In order to compare the collision avoidance effects of the two controllers, the distances between satellites and space obstacles are shown in Fig. 17 and Fig. 18. The distances between satellites in cluster are shown in Fig. 19 and Fig. 20. And the distances between satellites and target spacecraft are shown in Fig. 21 and Fig. 22.

In general, the satellite cluster achieves collision avoidance completely under the action of both controllers. However, by comparing the simulation diagrams, it can be found that the collision avoidance actions of RDMPC controller are more precise due to its ability to predict

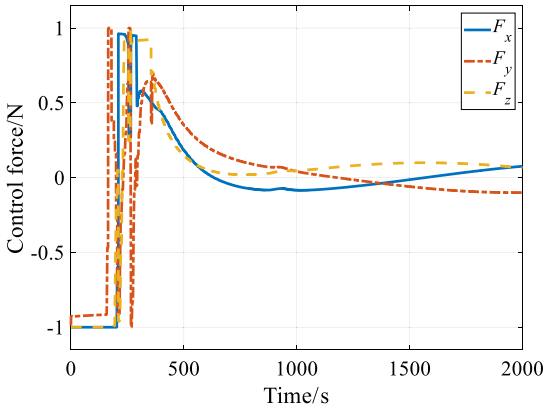

Fig. 23. The control force curves in three coordinate axes of Sat 1 under RDMPC controller.

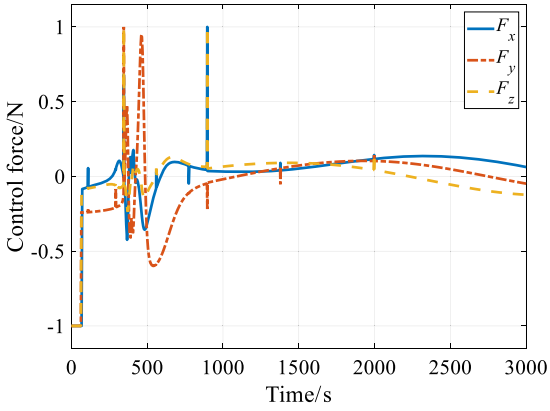

Fig. 24. The control force curves in three coordinate axes of Sat 1 under artificial potential field controller.

the future states of the satellites. On the contrary, the collision avoidance of the artificial potential field method controller is realized based on the setting of the repulsive potential field, which has a certain conservativeness.

Finally, the control force curves provided by the two controllers during the reconfiguration process are shown in Fig. 23 and Fig. 24.

It can be found in Fig. 23 and Fig. 24 that the amplitude of both controllers does not exceed the thrust constraint $T_{\max} = 1$ N. For collision avoidance control, there are many spikes in the control force curves when the artificial potential field method controller performs collision avoidance actions. While the control force curves of the RDMPC controller are smoother.

In summary, the numerical simulations show that the RDMPC strategy of satellite cluster designed in this paper can accomplish the task requirements of targets tracking and collision avoidance. Firstly, the RDMPC controller can adapt to different initial states of the satellites and the control effectiveness is verified. Then, by designing reasonable controller parameters, the RDMPC controller can achieve target tracking and collision avoidance under the condition of satisfying thrust constraints, and the fuel consumption of the satellites can be reduced at the same time. It is worth noting that the design of the slack variable ensures the feasibility of the controller and greatly simplifies the design difficulty of the terminal control law. Moreover, the Tube-based auxiliary controller can compensate the uncertain disturbance quickly and make the system have strong robustness. In addition, compared with the classical collision avoidance control method, the convergence rate and accuracy of the RDMPC controller are higher, and the control of collision avoidance is less conservative. However, the proposed method does not consider the communication delay between satellites and the computation time of each step of the RDMPC controller which may cause the information between satellites to be out of synchronization and affect the control effect of the controller. And this issue can be addressed in future studies.

5. Conclusion

In this article, a RDMPC strategy for reconfiguration of satellite cluster was developed. In view of multiple disturbances in space, a tube-based auxiliary controller was designed to compensate the control force. In this way, the errors between the actual and nominal states of the satellites can be kept within a quite small range related to the upper bound of the disturbances. Then a DMPC controller was proposed for the nominal system which can make the satellites track the targets without collision during the overall migration. Fuel consumption and evasive action can be decreased by adopting target allocation strategy based on Hungarian algorithm during the process of the reconfiguration mission. Through theoretical proof and numerical simulations, it can be concluded that each satellite can track its own target with high accuracy while the thrust constraints and collision avoidance were satisfied. In summary, the proposed control strategy was provided with good stability and robustness and can be applied to engineering practice.

Declaration of competing interest

The authors declare that they have no known competing financial interests or personal relationships that could have appeared to influence the work reported in this paper.

Data availability

No data was used for the research described in the article.

Acknowledgements

This work was supported by the the National Natural Science Foundation of China under Grant 62073102 and 62203145, and the National Key R&D Program of China under Grant 2021YFC2202900.

References

[1] Z. Zheng, J. Guo, E. Gill, Distributed onboard mission planning for multi-satellite systems, Aerosp. Sci. Technol. 89 (2019) 111–122.
[2] H. Zhang, P. Gurfil, Distributed control for satellite cluster flight under different communication topologies, J. Guid. Control Dyn. 39 (3) (2016) 617–627.
[3] J. Wang, C. Zhang, J. Zhang, Analytical solution of satellite formation impulsive reconfiguration considering passive safety constraints, Aerosp. Sci. Technol. 119 (2021) 107108.

[4] H. Zhang, P. Gurfil, Cooperative orbital control of multiple satellites via consensus, IEEE Trans. Aerosp. Electron. Syst. 54 (5) (2018) 2171–2188.
[5] C. Peng, S. Zhao, J. Li, et al., Provision of traffic grooming for distributed satellite cluster networks, Int. J. Satell. Commun. Netw. 38 (6) (2020) 557–574.
[6] M.K. Ben-Larbi, K.F. Pozo, T. Haylok, et al., Towards the automated operations of large distributed satellite systems. Part 1: review and paradigm shifts, Adv. Space Res. 67 (11) (2020) 3598–3619.
[7] F.Z. Cui, C.Q. Zhong, X.K. Wang, et al., A collaborative design method for satellite module component assignment and layout optimization, Proc. Inst. Mech. Eng., Part G, J. Aerosp. Eng. 233 (15) (2019) 5471–5491.
[8] S. Sarno, J. Guo, M. D'Errico, et al., A guidance approach to satellite formation reconfiguration based on convex optimization and genetic algorithms, Adv. Space Res. 65 (8) (2020) 2003–2017.
[9] G. Di Mauro, D. Spiller, S.F. Rafano Carnà, et al., Minimum-fuel control strategy for spacecraft formation reconfiguration via finite-time maneuvers, J. Guid. Control Dyn. 42 (4) (2019) 752–768.
[10] H. Liu, Y. Tian, F.L. Lewis, et al., Robust formation flying control for a team of satellites subject to nonlinearities and uncertainties, Aerosp. Sci. Technol. 95 (2019) 105455.
[11] A. Capannolo, M. Lavagna, Adaptive state-dependent Riccati equation control for formation reconfiguration in cislunar space, J. Guid. Control Dyn. 45 (5) (2022) 982–989.
[12] Z. Wang, Y. Xu, C. Jiang, et al., Self-organizing control for satellite clusters using artificial potential function in terms of relative orbital elements, Aerosp. Sci. Technol. 84 (2019) 799–811.
[13] Y. Xu, Z. Wang, Y. Zhang, Bounded flight and collision avoidance control for satellite clusters using intersatellite flight bounds, Aerosp. Sci. Technol. 94 (2019) 105425.
[14] M.A. AlandiHallaj, N. Assadian, Multiple-horizon multiple-model predictive control of electromagnetic tethered satellite system, Acta Astronaut. 157 (2019) 250–262.
[15] S. Zhu, R. Sun, J. Wang, et al., Robust model predictive control for multi-step short range spacecraft rendezvous, Adv. Space Res. 62 (1) (2018) 111–126.
[16] T. Pippia, V. Preda, S. Bennani, et al., Reconfiguration of a satellite constellation in circular formation orbit with decentralized model predictive control, arXiv preprint, arXiv:2201.10399, 2022.
[17] D. Menegatti, A. Giuseppi, A. Pietrabissa, Model predictive control for collision-free spacecraft formation with artificial potential functions, in: 2022 30th Mediterranean Conference on Control and Automation (MED), IEEE, 2022, pp. 564–570.
[18] C. Zagaris, H. Park, J. Virgili-Llop, et al., Model predictive control of spacecraft relative motion with convexified keep-out-zone constraints, J. Guid. Control Dyn. 41 (9) (2018) 2054–2062.
[19] R.R. Nair, L. Behera, Robust adaptive gain higher order sliding mode observer based control-constrained nonlinear model predictive control for spacecraft formation flying, IEEE/CAA J. Autom. Sin. 5 (1) (2016) 367–381.
[20] L. Sauter, P. Palmer, Analytic model predictive controller for collision-free relative motion reconfiguration, J. Guid. Control Dyn. 35 (4) (2012) 1069–1079.
[21] Y. Lim, Y. Jung, H. Bang, Robust model predictive control for satellite formation keeping with eccentricity/inclination vector separation, Adv. Space Res. 61 (10) (2018) 2661–2672.
[22] D. Morgan, S.J. Chung, F.Y. Hadaegh, Model predictive control of swarms of spacecraft using sequential convex programming, J. Guid. Control Dyn. 37 (6) (2014) 1725–1740.
[23] Z. Shi, F. Zhao, X. Wang, et al., Model predictive control-based mission planning method for moving target tracking by multiple observing satellites, in: 2022 IEEE 6th Information Technology and Mechatronics Engineering Conference (ITOEC), vol. 6, IEEE, 2022, pp. 1158–1162.
[24] D. Morgan, S.J. Chung, L. Blackmore, et al., Swarm-keeping strategies for spacecraft under J_2 and atmospheric drag perturbations, J. Guid. Control Dyn. 35 (5) (2012) 1492–1506.
[25] S. Yu, M. Reble, H. Chen, et al., Inherent robustness properties of quasi-infinite horizon nonlinear model predictive control, Automatica 50 (9) (2014) 2269–2280.
[26] J. Lofberg, Approximations of closed-loop minimax MPC, in: 42nd IEEE International Conference on Decision and Control (IEEE Cat. No. 03CH37475), vol. 2, IEEE, 2003, pp. 1438–1442.
[27] D. Limón, I. Alvarado, T. Alamo, et al., Robust tube-based MPC for tracking of constrained linear systems with additive disturbances, J. Process Control 20 (3) (2010) 248–260.
[28] D.Q. Mayne, E.C. Kerrigan, E.J. Van Wyk, et al., Tube-based robust nonlinear model predictive control, Int. J. Robust Nonlinear Control 21 (11) (2011) 1341–1353.
[29] D.Q. Mayne, E.C. Kerrigan, P. Falugi, Robust model predictive control: advantages and disadvantages of tube-based methods, IFAC Proc. Vol. 44 (1) (2011) 191–196.
[30] A. Nikou, D.V. Dimarogonas, Decentralized tube-based model predictive control of uncertain nonlinear multiagent systems, Int. J. Robust Nonlinear Control 29 (10) (2019) 2799–2818.
[31] J. Munkres, Algorithms for the assignment and transportation problems, J. Soc. Ind. Appl. Math. 5 (1) (1957) 32–38.
[32] Y. Guo, J. Zhou, Y. Liu, Distributed Lyapunov-based model predictive control for collision avoidance of multi-agent formation, IET Control Theory Appl. 12 (18) (2018) 2569–2577.
[33] J. Hwang, J. Lee, C. Park, Collision avoidance control for formation flying of multiple spacecraft using artificial potential field, Adv. Space Res. 69 (5) (2022) 2197–2209.